Mechanical Characterization of the Braided Composite Yarn and Bond Strength Evaluation of the Joints of the Open-Architecture Composite Structure (O-ACS)

by

Nakul Ajit Kothari

A thesis submitted to the Graduate Faculty of
Auburn University
in partial fulfillment of the
Requirements for the Degree of
Master of Science

Auburn, Alabama
August 2, 2014

Keywords: braiding, carbon fiber, composites, lattice structures, minimal weight structures

Approved by

David G. Beale, Chair, Professor of Mechanical Engineering
Royall Broughton, Jr., Professor of Polymer and Fiber Engineering
James Davidson, Professor of Civil Engineering

Abstract

Open-architecture composite structures (O-ACS) can be seen as structures, optimized for weight, meant to be used as beams or columns, in applications where the stiffness to weight ratio of the structure governs the design. The transversely isotropic, braided composite yarn that is used to make O-ACS in tube form is important in making them light and strong. Characterization of this yarn's mechanical properties was the goal of this study. Young's modulus along the axis was found using uniaxial tensile testing. Modulus along the transverse axis was found by performing transverse compression test and using Hertzian-contact model. Poisson's ratio was found using an image processing technique. Flexural modulus was found by performing a 3 point bend test and shear modulus was found using micromechanical modeling. Young's modulus, Poisson's ratio and shear modulus have also been calculated using the micromechanical model and good correlation was observed between the values found experimentally and from the micromechanical model.

The bond strength of joints formed by these yarns is also an important property that would govern the progressive developments of the yarn in order to make lighter and stiffer tubes. Mode 1 type of debonding of the joints has been studied and experimental techniques for finding the maximum load to failure of the joints have been developed. Four yarns with different jacket architectures have been tested and compared on the basis of their mechanical properties and bond strength of the joints formed. Our initial work towards simulating the mode 1 and mode 2 type of debonding of the joints using finite element software and cohesive zone modeling approach, in particular, has been reported.

Acknowledgements

I would like to thank my parents and elder brother for making my goal of pursuing higher education possible. You all have endured much for my wellbeing and cannot thank you all enough for that. I would like to thank Raja Uncle and Vikram Uncle to have financially helped me for my stay in USA so far. Without your support this would not have been impossible.

I must thank Dr. Beale for keeping much valued faith in me and being extremely patient all throughout the last 2 years. Being a TA for Senior Design Projects has taught me a lot and given me much more exposure to varied fields of mechanical engineering. You have helped me out at all stages of my research and also helped me get admission to the Doctoral Program at Auburn University. Thank you for giving me all the freedom to align my own career goals with research objectives and course work. I would also like to thank Dr. Davidson, under whom I did my most vital courses on Finite Element Method. I must thank him for the valuable guidance and for taking time out for being on my thesis defense committee.

I must also thank Dr. Broughton for his invaluable contributions towards my research. He is, as quoted by Dr. David Branscomb "a natural born problem solver". He has given me much knowledge and exposure, by taking me to the conferences where I did not even present, by creating opportunities time and again to help me in my goal to publish a technical paper. It has indeed been a great experience pursuing research under your guidance.

I would like to thank Austin Gurley for his invaluable help all throughout my research. He has been the 'go to guy' for me and I do aspire to strive for excellence the way he does in whatever tasks he undertakes. Dr. Branscomb has been a constant source of sound advice. I must thank Sanyam Shirgaonkar, Yeng Shen and Shane Furlong. Have learnt much from them and they have

been great to work with. I must also thank Amith Jain and Bala Murugan whose help I have sought not only in course work but also for my research.

Shantanu Deshpande, Bharath Ramakrishnan and Ravi Shankar Mahadevan have been the perfect roommates I could have asked for at the vital beginning of my life as a graduate student. I have learnt a lot from you all and am truly blessed to have you all as my close friends. I must thank Jasma Shukla and Ajit Chavan to have relieved of my duties in Indian Students Association committee when I needed the much vital time to complete my Thesis. I would also like to thank Robin Gautham Muthukumar for all the help in editing my manuscripts. I would also like to thank all my committee members of ISA.

Lastly, I would like to thank Pravina Masi, Shankar Masaji, Asit, Rima, Tina Ben,Raju Mama, Sachi and Jayesh to have been my close Family in this country . Coming to Houston and Charlotte at the end of every semester, and spending time with you all, has recharged me to work harder every time. Without your company and support this experience would have been much less exciting. Thank you all.

Table of Contents

List of Tables

List of Figures

x

Chapter 1 Introduction and Literature Review

Introduction

Need for lightweight structures are rapidly increasing in all fields of engineering. Ever since the development of mass production of composite materials, in spite of being relatively more expensive, usage of these materials has rapidly increased. These materials are predominantly used in the aircrafts and high performance automobiles to make chassis, body parts, flooring, etc as well as civil engineering structures and space satellites.

These materials are being used extensively for their high strength to weight and stiffness to weight ratio. Some of the most popular materials being used in the industry currently are carbon fiber reinforced plastic and glass fiber reinforced plastic. These two are available in the forms of woven Matts, roving, pultruded rods, chopped-strand Matts, etc. Development of innovative, repeatable manufacturing processes to produce these materials has made them less expensive than the other similar high modulus fibers like boron. Braiding has been one process which has been extensively used in the textile industry. With advancements in computer controlled machinery, fabrics with endless possibilities of permutations and combinations can be mass produced on these machines.

Braided sleeves of carbon fiber, glass fiber, Kevlar^{TM}, etc. have been sold in the market for several years now. Researchers in the past have also braided the tows of these fibers on a mandrel and cured them, resulting in an open truss structures [2].

Overview of Previous Work

Researchers from Auburn University have in the past developed a novel method of making open lattice structures or open architecture composite structures as shown in Figure 1 .These structures were made by braiding a yarn, made of a bundle of prepreg carbon fiber tows covered with a braided jacket of textile fiber.

Figure 1: Open architecture composite structures in the past [2]

Several aspects of these tubes were studied. Developing a novel manufacturing method required a thorough understanding of the braiding technology. Lace braiding technology was explored initially as a solution to engineer pattern controlled braided structures [2]. Lace braiding technology allows the user to control each yarn individually which made it one of the most versatile technology solutions in braiding [3]. Traditional horizontal maypole braiding machine was used next when the lace braiding technology was found to not give desirable results. After many efforts, a horizontal maypole braiding machine was found to work well. A novel jacket architecture called the true tri axial weave was successfully made on a horizontal braiding machine [2]. This jacket architecture was later found to be the most efficient architecture for a braided composite yarn.

Tensile modulus and tensile strength of the braided yarn were found experimentally [2]. Flexural modulus was found by 3 point bend test. Nondestructive testing methods like infrared thermography was used to evaluate damage in the tubes which were subjected to 3 point bend test [5]. Shear modulus of tubes under torsion loads was also found experimentally and verified using finite element methods [1].

Detailed CADS models representing geometry of the braided tubes were developed. Detailed ground work was laid prior to this study to understand the potential, importance and impact of the open architecture composite tubes in the industry.

Prior to the efforts of our research team. Open lattice composite structures have been developed by other researchers. These similar projects include the Iso truss, developed by researchers in Brigham Young University [8], Utah and an open lattice pyramid structures by researchers in Virginian Tech University [9], as shown on in Figure 2 .
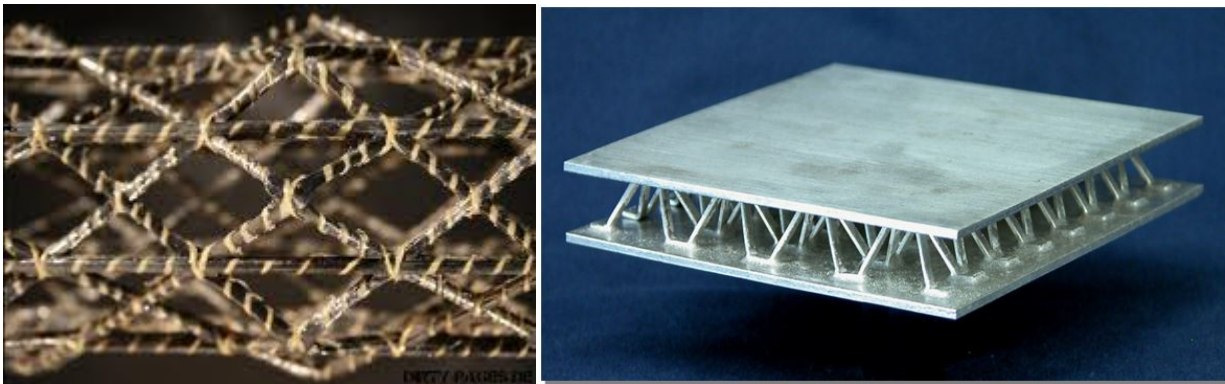
| (a) | (b) |

Figure 2: (a) Isotruss, (b) Open lattice composite pyramidal structure

From the initial literature review of the prior work done in these tubes, one of the important conclusions was the need to improve the yarn to improve the performance of the tube under various types of loading conditions. The work presented in this study is our efforts in understand the yarns from a mechanical engineering point of view and improving them. It is also a secondary goal of this study to understand the micro strength of the joints formed by these yarns and effect of joint strength on the performance of the O-ACS.

Overview of Yarn Manufacturing

Introduction

Open architecture tubes are made by over braiding the composite yarn on a mandrel that serves as a preform [3]. Both the tube and the yarn are made on a horizontal braiding machine. The composite yarn is a hybrid, with the core made of a high modulus fiber for strength purposes and a braided jacket, surrounding the core, made of textile fiber for improved braid ability [2]. The core is made of prepreg high modulus fibers like carbon fiber. This prepreg tow, apart from the

strength advantages, has a disadvantage that it is sticky and thus does not have good braid ability. It is the jacket of the yarn that improves the braid ability of the yarn. It also protects the yarn from foreign media and protects the yarn from damage while braiding. Most importantly it is found to consolidate the yarn cross section and increase the packing density of the cross section.

Manufacturing Process

Figure 3 [2] shows a horizontal braiding machine and the yarn made by the machine. Figure 3 is a schematic of the setup showing the horizontal braiding machine, take-up mechanism and the stand at the back that holds the spools of prepreg tow.
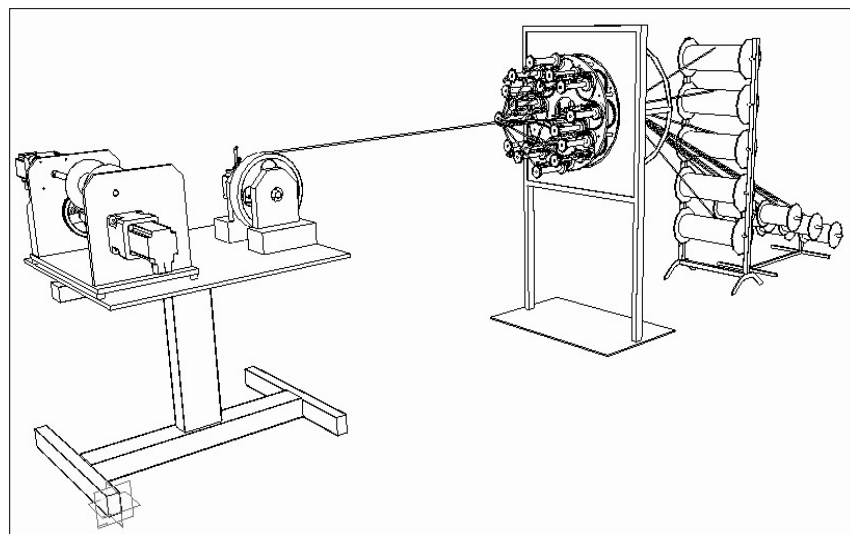
Figure 3 : Horizontal braiding machine and take-up mechanism

A computer with software that controls a motor that governs the take-up speed of the yarn being made [4] was used previously to set the take-up speed.

Pioneering work on the manufacturing the yarn was done by researchers from our team, in the past. Yarns of different jacket architectures were tested to understand the effect of jacket on the core [2]. Damage in the yarns of an open architecture tube was studied using non-destructive testing schemes [5]. In this study, the aim of the research has been to better understand the yarn from the perspective of its mechanical properties. For this purpose, yarns with same core, similar jacket architecture but different types of textile fiber (of varying denier count), and different amounts of carbon fiber (prepreg or dry) in the jacket have been studied. Four types of yarn were made.

4

Table 1 shows the composition of each type of yarn.

Table 1 : Yarns and their composition

	#1	#2	#3	#4
Core	48 K T700 prepreg	48 K T700 prepreg	48 K T700 prepreg	48 K T700 prepreg
Jacket Helicals (clockwise)	4 X 400 D Polyester	4 X 400 D Kevlar^{TM}	4 X 1000 D nylon (carpet yarn)	4 X 400 D nylon (carpet yarn)
Jacket Helicals (anticlockwise)	4 X 400 D Polyester	4 X 400 D Kevlar^{TM}	4 X 1000 D nylon (carpet yarn)	4 X 400 D nylon (carpet yarn)
Jackets Axials	4 X 3K T300 prepreg 4 X 3K T300 dry	4 X 3K T300 prepreg 4 X 3K T300 dry	8 X 3K T300 prepreg	4 X 400 Vectran^{TM}

 The yarns mentioned in Table 1 were manufactured and tested for different mechanical properties. A detailed process flow of the manufacturing of the yarns is shown below. The yarns made, were cut to a length of 30 cm and cured for 3 hours at 125^{0}C, while being clamped with in a fixture, for maintaining them straight and with least amount of twist. The properties of the prepreg core and resin were used from the respective datasheets [6][7].
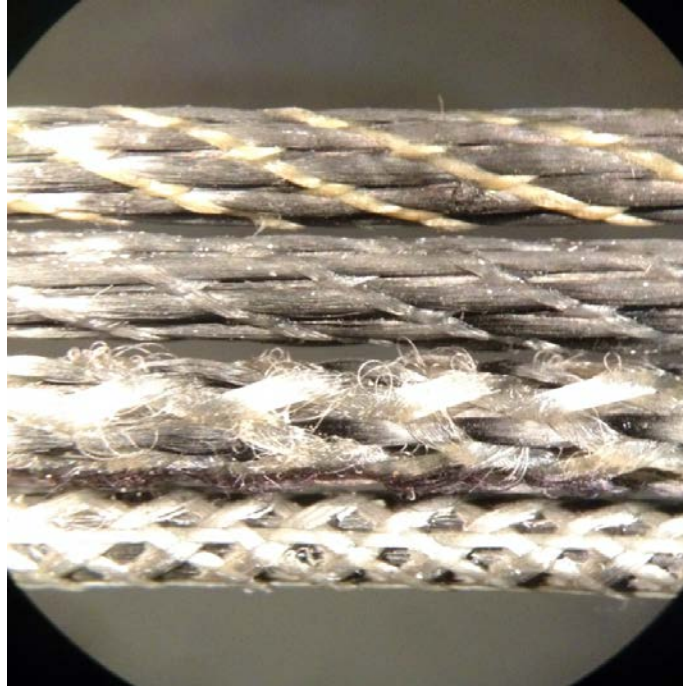
Figure 4: Yarns #1, #2, #3 and #4 (from top to bottom)

Figure 4 shows the yarns of different jacket architectures mentioned in Table 1. The braid angle of the helical yarns is governed by the Equation 1.

$$\alpha = \tan^{-1}(\frac{\omega r}{v})$$ Equation 1

Decide on core size and type of fibers for the core and the jacket

1
- Depending on the application, decide on core size .
- 36 K / 48 K high modulus prepreg fiber tow

2
- Textile fiber as helicals in the jacket
- Example: kevlar, nylon, vectran of a particular denier count

3
- Prepreg /dry high modulus fiber as axials in the jacket
- Example : 3K T300 prepreg/dry, 3K glass fiber prepreg

Setup the braiding machine

4
- Setup the prepreg tows at the back of the braiding machine

5
- Wind the textile fibers on the bobbins

6
- Setup the bobbins with the helical fibers for the jacket, on the appropriate carriers on the front side of the machine

7
- Setup the bobbins/ spools with axial fibers of the jacket, on carriers at the backside of the machine

Set the parameters for braiding process

8
- Decide on the braid angle required
- Example: 22.5, 33.75, 45 (angle in degrees)

9
- Using (1), find the correct combination of angular velocity and take up speed that results in the required braid angle

10
- Set the angular velocity for the braiding machine
- Set the velocity for the take-up machine

Make yarn

11
- Watch the braiding machine and the take-up machine carefully while the yarn is being braided

12
- Replace/refill the bobbins/spools once the fibers on them are used up

13
- Cut lengths of yarn required on each bobbin , for making the open architecture tube
- Wind the yarn on to the bobbins

Material Characterization

Composite materials are non-homogenous materials. This non homogeneity, results in behavior of the material being dependent on the load and the manner in which the load is applied. Thus these materials have a larger number of unique constants than the homogenous metals. To find the number of unique constants that would fully define a given composite it is necessary to categorize it amongst one of several types of non-homogeneities. Following are the types:

1. General Anisotropic materials

These materials have symmetry present. There are 21 independent constants that define the material [10].

2. Monoclinic materials

These materials have one plane of symmetry. This one plane of symmetry reduces the number of independent constants from 21 to 13 [10].

3. Orthotropic materials

These materials have 3 mutually perpendicular planes of symmetry. These materials have 9 independent constants. A single ply unidirectional laminate is an example of orthotropic materials [10].

4. Transversely orthotropic

These materials have one plane of material symmetry and also the mechanical behavior along that plane is the same everywhere and thus isotropic in one direction. There are 5 independent elastic constants for such a material. A multilayered unidirectional composite sheet is an example of this [10].

The braided yarn is made of multiple layers of prepreg tows as shown in fig and is thus similar to a transversely isotropic material.

Equation 2 shows the simplified strain-stress relationship matrix [10].

$$
\begin{bmatrix} \epsilon 1 \\ \epsilon 2 \\ \epsilon 3 \\ \gamma 23 \\ \gamma 13 \\ \gamma 12 \end{bmatrix} = \begin{bmatrix} 1/E1 & -v12/E1 & -v31/E1 & 0 & 0 & 0 \\ -v12/E1 & 1/E1 & -v31/E1 & 0 & 0 & 0 \\ -v13/E1 & -v13/E1 & 1/E3 & 0 & 0 & 0 \\ 0 & 0 & 0 & 1/G13 & 0 & 0 \\ 0 & 0 & 0 & 0 & 1/G13 & 0 \\ 0 & 0 & 0 & 0 & 0 & 2(1+v12)/E1 \end{bmatrix} \begin{bmatrix} \sigma 1 \\ \sigma 2 \\ \sigma 3 \\ \tau 23 \\ \tau 13 \\ \tau 12 \end{bmatrix}
$$

Equation 2

In the Chapters to come we have found Young's modulus along the axis (E_L), modulus along the transverse axis(E_T), major Poisson's ratio (v_{LT}) and torsion modulus (G_{LT}). Flexural modulus of the yarns and load to failure for the joints formed by the yarns are also reported.

References

1. D. Branscomb, A. Gurley, D. Beale, R. Broughton, "Open-Architecture Composite Tube Design and Manufacture" *ASME Early Career Technical Journal*, 2012

2. D.Branscomb, " Minimal Weight Composites Utilizing Advanced Manufacturing Techniques ", PhD dissertation, Auburn University, 2012

3. Head, A., F. Ko, and C. Pastore. Atkins and Pearce Handbook of Industrial Braiding. Covington: Atkins and Pearce, 1989.

4. Beale, D., D. Branscomb, and R. Broughton. "Application of and System Examination of Braid." *ASME 2010 International Design Engineering Technical Conferences*, Computers and Information in Engineering Conference Machine Vision Techniques for Fault Diagnostics IDETC/CIE 2010. Print.

5. D. Branscomb, I. Cerkez, "Damage Evaluation of Braided Kevlar®/Carbon/Epoxy Composite Beams in Three Point Bending with Infrared Thermography", *2010 ASME Early Career Technical Journal* (2010)

6. T700S Technical Data Sheet

7. U3325 TCR^{TM} Technical Data Sheet

8. Gregory Larson, David Jensen ,"Transverse Loading of a Graphite/Epoxy Iso Truss Panel",*47th AIAA/ASME/ASCE/AHS/ASC Structures, Structural Dynamics, and Materials Conference*

9. Kevin A. Finnegan, "Carbon Fiber Composite Pyramidal Lattice Structures", Master Thesis, University of Virginia, 2007

10. Dr. Jeffrey Suhling, "Mechanics of Composite Materials: Volume 1" , MECH 7360,2013, pg 135

Chapter 2 Young's modulus along the axis

Introduction

Open architecture tubes are made of braided yarns, some running along the axis and some revolving around the axis in a helical path as shown in Figure 5 .The behavior of the tube under tensile loads, the flexural stiffness of the tubes and behavior under buckling loads are dependent on tube geometry and yarn stiffness. Tube stiffness is directly dependent on the stiffness properties of the yarn. Mathematically, the axial components of the stiffness for the yarns along the axis and the yarn along the helical path can be added up by the theory of superposition to form the global stiffness matrix of the tube [2].
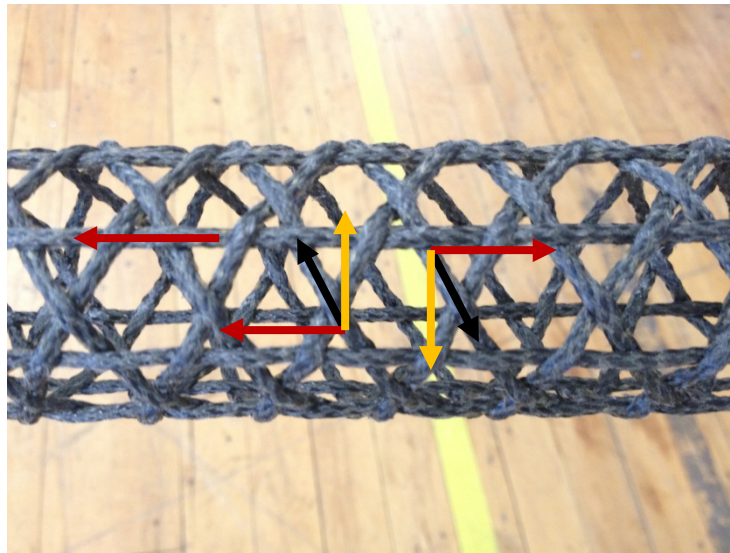
Figure 5 : Tube with axial and helical yarns marked for the stiffness

Because of this direct relevance of the strength of the axial yarn to the strength of the tube, it is very important to study the properties of the braided yarn. For this study, uniaxial tensile tests on

the yarns were done to find the Young's modulus along the axis. Yarns with different jacket architectures (Table 2), with diameter ranging between 2 to 3 mm were studied over the course of this research. Thus, for doing tensile tests, the braided yarn can be tested in a manner similar to testing thin metal wires, ropes, and filaments of textile fibers. All these three were found to be similar to the braided yarns in of their geometrical attributes.

Table 2: Yarns and their composition

	#1	#2	#3	#4
Core	48 K T700 prepreg	48 K T700 prepreg	48 K T700 prepreg	48 K T700 prepreg
Jacket Helicals (clockwise)	4 X 400 D Polyester	4 X 400 D Kevlar^{TM}	4 X 1000 D nylon (carpet yarn)	4 X 400 D nylon (carpet yarn)
Jacket Helicals (anticlockwise)	4 X 400 D Polyester	4 X 400 D Kevlar^{TM}	4 X 1000 D nylon (carpet yarn)	4 X 400 D nylon (carpet yarn)
Jackets Axials	4 X 3K T300 prepreg 4 X 3K T300 dry	4 X 3K T300 prepreg 4 X 3K T300 dry	8 X 3K T300 prepreg	4 X 400 Vectran^{TM}

Researchers in the past have studied tensile behavior of wires [2]. Tensile tests on single filaments have been done [1,7]. Researchers have also performed tensile tests on three dimensional braided composite structures [4,5] .The most popular method for performing the tensile tests is the usage of universal tensile testing machine. ASTM Standards for tensile testing of the single textile fiber [8] and high modulus single filament materials [9] were consulted. No standard test procedures have been made for thin cylindrical composites, similar to the braided yarn. This meant that a new test would have to be designed for these yarns. These

aforementioned ASTM standards gave several insights to design a tensile test for the braided yarn.

Test Setup

From the literature review it was decided that the braided yarn would be clamped directly into the clamps of the UTM. In order to get the Young's modulus, the yarn would be loaded within its elastic limits. As per the ASTM standards, the gauge length of the tensile test specimen should be equal to or more then 1.5 to 4 times the width of the specimen [10]. Since the yarn has a very small diameter, the gauge length of the specimen during the tests did not pose any difficulty. In the past, researchers from our team have tested the yarn with end caps as shown in Figure 6.

(a)   (b)

Figure 6 : Tensile test sample with(a) and without (b) end tabs

The yarn with potted end caps were made by potting room temperature cure epoxy resin in pipe fittings with the head drilled out for the yarn to go in. The yarn in Figure 6 was clamped within the pneumatic grips of the Universal Tensile Machine (UTM) as shown in the Figure 7. Data could be recorded in two ways. The first method was using an extensometer based on rotation of lead screws in the load frame and the second was a video extensometer connected to the machine externally.

Video Extensometer

The working principle of the video extensometers is based on 2D digital image correlation. A full view camera records the digitized image of the sample before the loading starts. Care has to be taken to see that the distance between the camera and the specimen remains constant during

the test. Also, constant illumination is achieved by having a separate source of illumination as shown in the Figure 7.
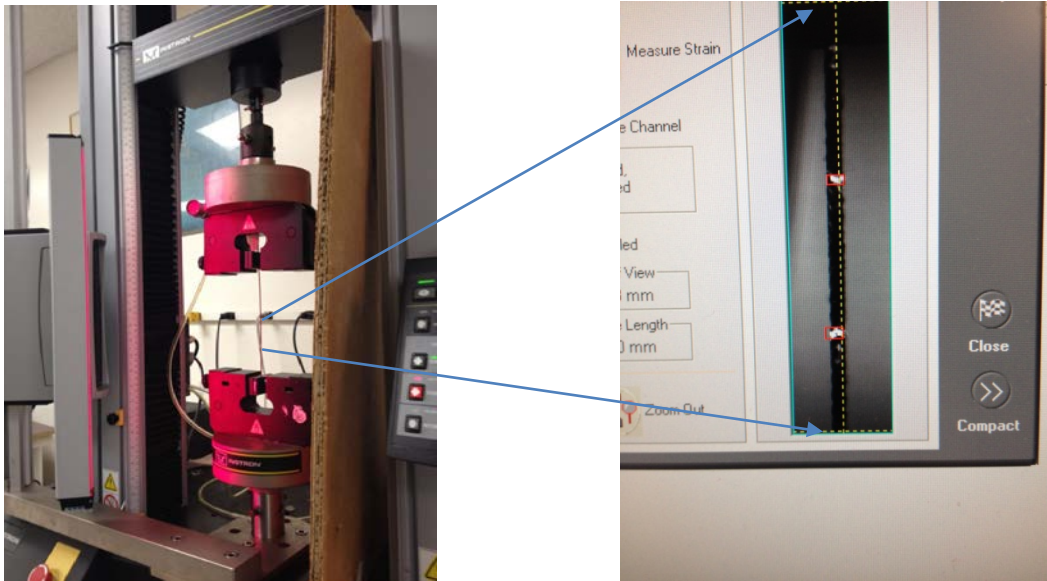
Figure 7 : tensile test strain data recording using video extensometer

Using white paint, markers were drawn on the surface of the specimen. The markers need to be distinctly sharp so that the contrast between the markers and the background ensure correct edge detection and tracking by the camera software. The target position is detected at the edge of a contrast transition and is hence not affected by changes in target width. The camera detects the markers put on the specimen and calculates the distance between the markers, thus giving the user the initial gauge length. Now as the test starts and the applied load causes deflections, the camera detects the changes in gauge length from frame to frame and converts into the displacement relative to the initial gauge length [21]. Since the displacement is calculated with respect to the initial gauge length and not the previous gauge length, the strain measured is the engineering strain and not true strain.

Method

The UTM was set to record the load and the deflection data. The UTM uses this data to generate a stress Vs strain graph using the formulae shown below [21]

Equation 3

$$\text{Stress}, \sigma = \frac{Load, L}{Area, A}$$

14

In our case, $\sigma = \frac{4L}{\pi d^2}$

For Young's modulus, the system uses a least square routine to construct a line between the bounds specified. It would interpolate the start and the end values if the values do not match the actual data points as shown in the Figure 8 [11].
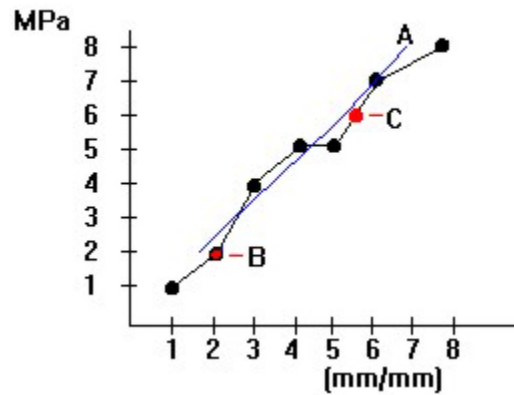
Figure 8 : Least squares fit for the data points

Dividing the tensile stress by the corresponding strain for each data point, Young's modulus is obtained [14] as shown in Equation 5.

Young's modulus, $Y= \dfrac{\dfrac{Load\ at\ point\ on\ tangent}{(original\ width)(original\ thickness)}}{\dfrac{elongation\ at\ point\ on\ tangent}{initial\ gauge\ length}}$

Figure 9 shows a detailed flowchart of the steps taken to find the Young's modulus of the braided yarn.
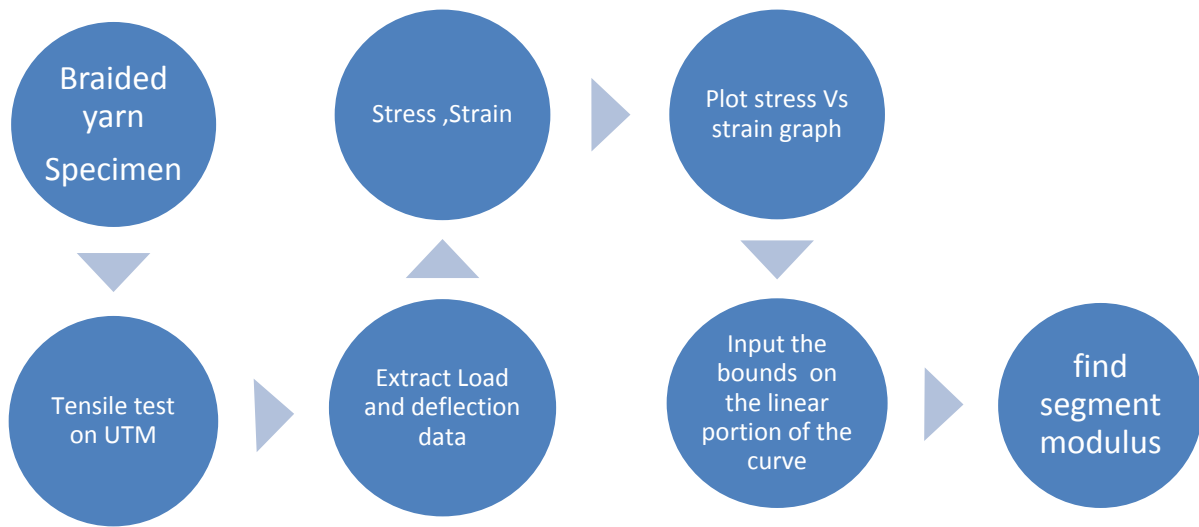
Figure 9 : Process flow for tensile modulus

Results

Four yarns of different construction, mentioned in the earlier section, were tested. It is important to note that all the different types tested had the same core of 48 K T700 tow. The difference was in the jacket. Yarn #1 and #2 had 8 X 400 denier Kevlar[TM] and 8 X 400 denier polyester fiber respectively. Both these yarns had 4 X 3K T300 prepreg tow and 4 X 3K T300 dry carbon fiber tow. Yarn #3 had 8 X 1000 denier tufted nylon in the jacket alongside 4 X 3K T300 prepreg tow. Yarn #4 had the 12 X 300 denier Vectran[TM] fiber in the jacket with no carbon fiber in the jacket. Thus #4 had the least amount of carbon fiber amongst the all the yarns tested (Table 1).

Load Vs axial strain (%) was plotted using the load and displacement data. This data was further used to plot the stress Vs strain graph. The stress Vs strain graph is usually plotted internally inside the machine to calculate the Young's modulus. Figure 10 shows a representative Load vs axial strain (%) graph for yarn #2.
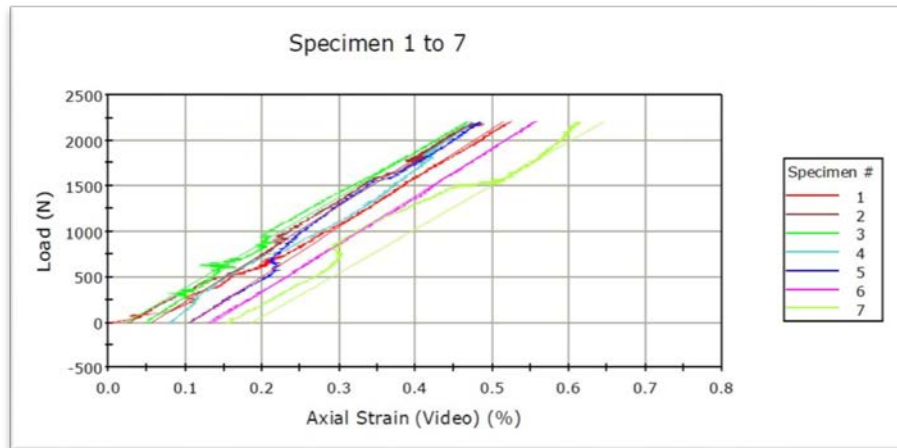
Figure 10 : Graph for load Vs axial strain for samples for the Young's modulus, Yarn #2

Similar graphs were obtained for the 4 types of yarns tested. Young's modulus was found for each of the 7 samples tested per yarn and results are listed in the Table 2

Table 3 : Young's modulus along the axis for different yarns

Yarn type / Sample number	E_L for #1 (GPa)	E_L for #2 (GPa)	E_L for #3 (GPa)	E_L for #4 (GPa)
1	101.61	117.57	111.49	97.17
2	113.88	121.13	110.64	86.85
3	104.82	104.53	96.57	107.47
4	130.63	115.73	136.62	119.37
5	116.73	104.86	108.21	96.82
6	122.07	124.121	108.43	90.49
7	113.92	118.46	117.93	85.178
Average	114.81	115.20	112.84	97.62
Standard Deviation	9.85	7.65	12.27	12.19
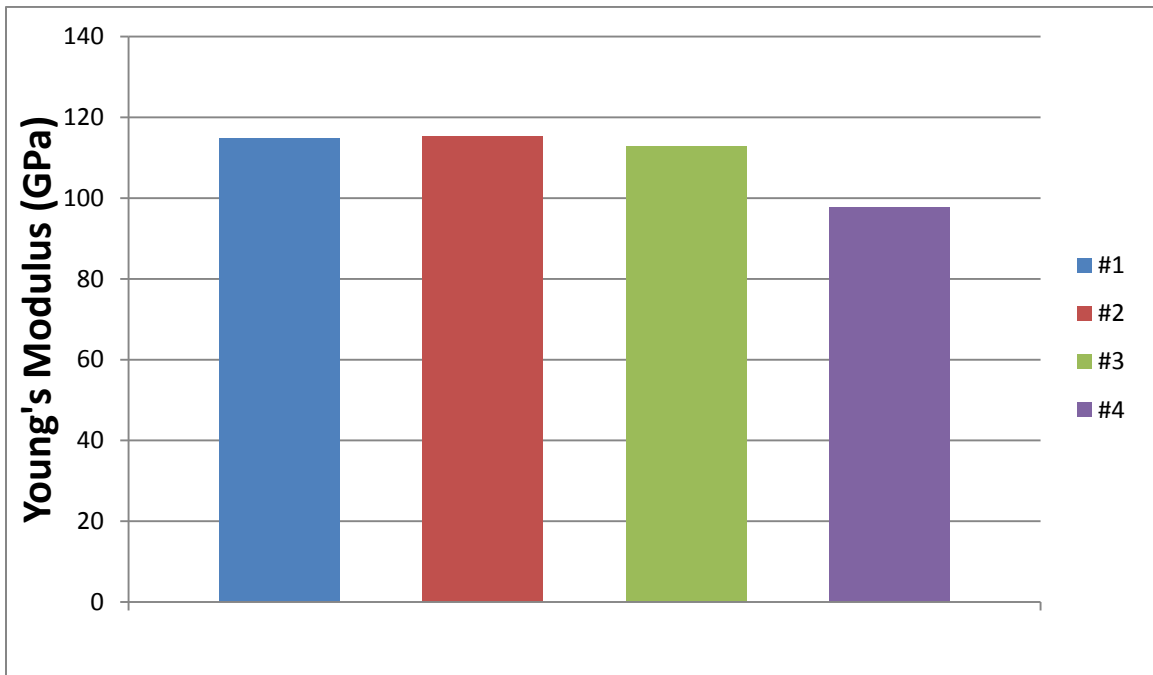
Figure 11: Comparison of Young's moduli for different yarns

Conclusion

Figure 11 shows the comparison of 4 yarns with respect to the averaged Young's moduli. From the Table 1 it can be seen that the yarns #1 and #2 have a very similar composition, the only difference being the type of textile fiber used in the jacket. They are found to have a near equal average Young's modulus. Yarn #4 has no carbon fiber tow in the jacket and thus the relatively low Young's modulus. Yarn #3 was found to have a higher value of Young's modulus than yarn #4 since it had more number of carbon fiber prepreg tows in comparison. It was found to have slightly lesser modulus than yarn #1 and #2. This was because of more number of carbon tows in yarn #1 and #2. Yarn #1 and #2 have 4 prepreg and 4 dry carbon fiber tows, whereas yarn #3 only has 4 prepreg tows in the jacket.

Though the Young's modulus of the yarn is an important property, it is worth noting that O-ACS tube made of yarn with high modulus may not have the highest tensile modulus in comparison to the O-ACS tubes made of the other 3 yarns. This was found from our work on the joint strength of the yarns, which is discussed in Chapter 6. The tensile modulus of the O-ACS tube depends not only on the tensile modulus of the joint but also on the strength of joints formed by the yarn. A pure tensile load on a tube would cause the axial and the helical yarns to extend. The helical yarns would have a tendency to straighten. The stiffness of the helical yarns along the axis of the tube would be less than that of the axial yarns. This mismatch would cause the joints to fail with mode 2 type of debonding. Thus it is worth noting that improving the tensile stiffness of the O-ACS tubes is dependent not only on the tensile modulus of the yarn but also on the stiffness of the joint along the tangent direction.

References

1. J.A. Bencomo-Cisneros, A. Tejeda-Ochoa, J.A. García-Estrada, C.A. Herrera-Ramírez, A. Hurtado-Macías, R. Martínez-Sánchez, J.M. Herrera-Ramírez, Characterization of Kevlar-29 fibers by tensile tests and nano indentation, *Journal of Alloys and Compounds*, Volume 536, Supplement 1, 25 September 2012, Pages S456-S459, ISSN 0925-8388

2. R.C. Hibbeler , Structural Analysis ,Fifth Edition, Chapter 13, pg 504

3. Ahmet Akdemir, Recai Kuş, Mehmet Şimşir, Investigation of the tensile properties of continuous steel wire-reinforced gray cast iron composite, *Materials Science and Engineering: A*, Volume 528, Issues 10–11, 25 April 2011, Pages 3897-3904, ISSN 0921-5093

4. Zixing Lu, Biao Xia, Zhenyu Yang, Investigation on the tensile properties of three-dimensional full five-directional braided composites, *Computational Materials Science*, Volume 77, September 2013, Pages 445-455, ISSN 0927-0256

5. Tomasz Brynk, Rafal M. Molak, Miroslawa Janiszewska, Zbigniew Pakiela, Digital Image Correlation measurements as a tool of composites deformation description, *Computational Materials Science*, Volume 64, November 2012, Pages 157-161, ISSN 0927-0256

6. Zixing Lu, Chengyu Wang, Biao Xia, Zhenyu Yang, Effect of interfacial properties on the uniaxial tensile behavior of three-dimensional braided composites, *Computational Materials Science*, Volume 79, November 2013, Pages 547-557, ISSN 0927-0256

7. D. Zhu, B. Mobasher, J. Erni, S. Bansal, S.D. Rajan, Strain rate and gage length effects on tensile behavior of Kevlar 49 single yarn*, Composites Part A: Applied Science and Manufacturing*, Volume 43, Issue 11, November 2012, Pages 2021-2029, ISSN 1359-835X

8. ASTM D3822-01, Standard Test Method for Tensile Properties of Single Textile Fibers

9. ASTM D3379-75e1, Standard Test Method for Tensile Strength and Young's Modulus for High-Modulus Single-Filament Materials, 1989

10. ASTM 3039 Test method for tensile testing of fiber resin composites

11. D.Branscomb, " Minimal Weight Composites Utilizing Advanced Manufacturing Techniques ", PhD dissertation, Auburn University, 2012

12. Instron^{TM} Bluehill Calculation Reference Version 1.1, Section on Segment modulus, pg 110

13. Standard Video Extensometer SVE 2663-82, Chapter 1, pg 1-7

14. IPC-TM-650 Test Methods Manual, Institute for Interconnecting and Packaging Electronic Circuits , pg 3

Chapter 3 Compressive Modulus, E_T and Flexural Modulus

Compressive Modulus in Transverse Direction

Introduction

 In this chapter transverse properties of the yarn are studied. Often, the open architecture tubes are subjected to bending and crushing (compressive) loads. In these loading scenarios the yarn undergoes diametric compression for a brief moment. The transfer of loads through the cross section of the yarn can be understood by finding the transverse modulus of the yarn. This is also necessary to understand the load transfer mechanisms through the joints of the tube, the compressive strength of the yarns, important for developing a method of connecting the open architecture tubes.

Extensive work has been done in the past on the axial properties of high modulus, highly oriented single fibers and bulk fibers. Little work has been on the transverse properties of these fibers. For highly oriented fibers, the ratio between axial and transverse elastic modulus has been found to be as high as 170 [1]. Kawabata et al have fully defined the compliance matrix for anisotropic high performance fibers based on their tests on single filaments [2]. Transverse properties of multiple fibers have been studied [1], researchers have done transverse compression tests on thick monofilaments [3]. Burgoyne and Brown have determined transverse properties of bulk of aramid fibers [4]. Transverse modulus for single filaments has been found with nano indentation [5]. Also the complexity involved in modeling a bulk of fibers under transverse compressive loads using finite element method is much more than that for modeling single yarns [13].

The braided yarn has a core made of 48K high modulus prepreg carbon T700. Approximate diameter of each filament is around 5-6 micrometer. It has been shown by the researchers in the past that properties of single fibers are not representative of the multiple fibers of the same kind [4]. This is because resin fills the spaces between fibers and air voids, packing density in the cross section and introduction of foreign particles during the process of manufacturing. Thus for this study all the tests were performed on the fully cured composite yarn instead of the single filaments as the properties of the bulk of fibers were of interest. Another reason for this was also that the braided yarn is an assembly of different kind of textile fibers and at different orientations in the jacket and the core and thus testing single fibers of each kind would not be representative of the final yarn.

The way the braided fibers are loaded and unloaded during the test is of prime importance. The modulus of the yarn measured while being loaded for the first time and the modulus measured after unloading and reloading of the same yarn can be different [4]. This is because of the re-adjustments and movement of the fibers on the top section of the yarn where the load is applied. The amount of spacing between filaments in the yarn and packing density are important properties that affect the behavior of yarn under compressive loads [13].The bulk of fibers would tend to get stiffer as the few initial loading cycles are applied. The elastic modulus is underestimated if the compressive load is causing a considerable amount of localized deformation. Thus it is important to make sure that the compressive load applied is distributed over an area and is not acting as a line load. Four types yarns with different jacket architectures were tested (Table 4).

Table 4: Yarns and their composition

	#1	#2	#3	#4
Core	48 K T700 prepreg	48 K T700 prepreg	48 K T700 prepreg	48 K T700 prepreg
Jacket Helicals (clockwise)	4 X 400 D Polyester	4 X 400 D Kevlar^{TM}	4 X 1000 D nylon (carpet yarn)	4 X 400 D nylon (carpet yarn)
Jacket Helicals (anticlockwise)	4 X 400 D Polyester	4 X 400 D Kevlar^{TM}	4 X 1000 D nylon (carpet yarn)	4 X 400 D nylon (carpet yarn)
Jackets Axials	4 X 3K T300 prepreg 4 X 3K T300 dry	4 X 3K T300 prepreg 4 X 3K T300 dry	8 X 3K T300 prepreg	4 X 400 Vectran^{TM}

Experimental Setup

A universal tensile testing machine, Instron^{TM} 5565 was used and a custom made loading device made of aluminum was used for loading the yarn. An aluminum cylinder with 73.5 mm diameter was used. The large diameter of the face would ensure that length over which the load would be applied is distributed over several fibers on the top surface and does not cause localized plastic deformations. The yarn was rested on a stiff steel plate and taped on to the surface to prevent the lateral movement and rolling of the yarn as shown in Figure 12 .
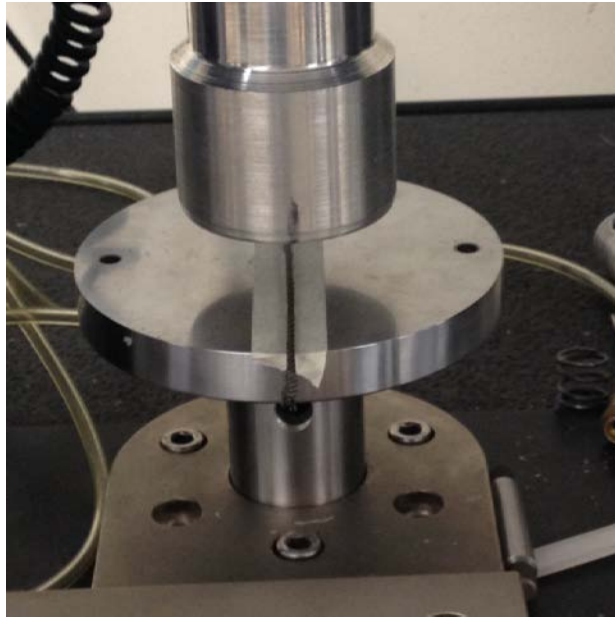
Figure 12 : Test fixture for transverse modulus test

In order to find the transverse modulus, a Hertzian-contact model, for the isotropic and transversely isotropic material was used. This Hertzian-contact model has been described briefly in the following section.

Hertzian Contact Model

Researchers in the past have used two kinds of methods for calculating the transverse moduli [6] of single filaments. Both the methods are based on Hertzian-contact problem of an isotropic cylinder compressed between two rigid, parallel platens. Some have modeled contact between the upper and lower plates as a distributed load [1] and some have modeled it as a line load at the bottom and distributed load at the top [3].Both the models have been found to give identical stress distributions [6,7]. Jawad and Ward's model results in equations simpler to fit the

experimental data and thus this model was used for our purpose. Jawad and Ward used a contact patch width of *2b*, shown in Figure 13.
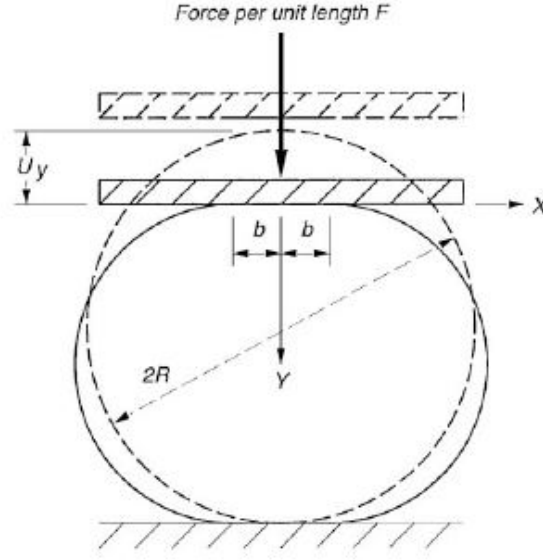
Figure 13 : loading condition and cross section for single fiber transverse compression test

$$b = \sqrt{\frac{4\,(\hat{s}_{11})(F)(R)}{\pi}}$$

Here, $\hat{s}_{11} = s_{11} - (s_{13})^2/s_{33} = 1/E_2 - (v_{12})^2/E_1$

In the equation above, since the value of E_1 is very large compared to v_{12} and square of v_{12} would be a very small number, the second term in Equation 5.

$\hat{s}_{11} \approx s_{11}$

Now from the Hertzian contact theory, Jawad and Ward simplified the load-deflection curve as follows

$$Uy = \frac{4(F)(\hat{s}11)}{\pi}[0.19 + \operatorname{arcsinh}(\frac{R}{b})]$$

This equation was further simplified using Equation 4 and Equation 7 as follows:

26

$$U_y = \frac{4(F)}{\pi(E2)} \left[0.19 + \operatorname{arcsinh} \sqrt{\frac{\pi(E2)(R)}{4F}} \right]$$

<div align="right">Equation 10</div>

Method of Calculations

Equation 9 is a nonlinear equation and thus MATLAB^{TM} was used to solve the equation. Function 'fzero' was used to solve the equation. This function is used to find roots to a nonlinear function. The function requires 2 arguments, for example *fzero (f(x), a)*. Here *f(x)* is the function with unknown roots and *a* is an initial best guess. The function 'fzero' tries to find the unknown root of the defined function that makes the function go to zero. Thus the solution is found where the defined function changes sign. Function '*fzero*' begins at *a* and tries to locate a point '*x*' where *f(x)* has the opposite sign of *f (a)*. Then function '*fzero*' iteratively shrinks the interval where *f(x)* changes sign to reach a solution [11].

The raw data of force, displacement and time was obtained from the tensile testing machine and processed to find the first derivative of the load and displacement, as done by researchers in the past [1,12]. This first derivative of the load and displacement was found simply by subtracting the current value of force at a data point from the value of the previous data point ie $f_2 - f_1$ and similarly $y_2 - y_1$. The Hertzian-contact model used, required the input of force in terms of force applied per unit length,[3,6] and thus the gradient of force obtained was divided by the length of yarn under the load. E_T was now found by fitting the data of first derivative of load and displacement to Equation 9.

Process Flowchart

Test the sample

Divide the first derivative of load data by the length of specimen

Plug in the processed data into the Hertzian-contact model

Collect raw data from UTM

Differentiate load and displacement data

Plot E_t Vs Time /Load/displacement

Find the maximum value of transverse modulus
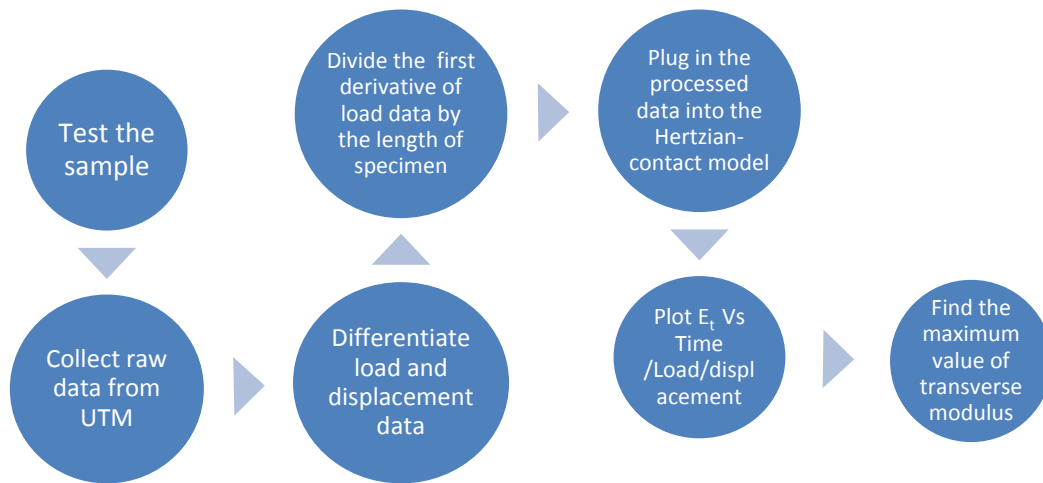
Figure 14: Process flow for finding E_T

Method Verification

It was important to verify the test setup, method and procedure before testing the braided yarns. This could be done by finding the transverse modulus of solid cylindrical composite tubes, of who's the value of transverse modulus would be known. Jawad and Ward had found the transverse modulus of nylon 6,6 , thin solid cylindrical rods using the Hertzian contact model for transversely isotropic materials.
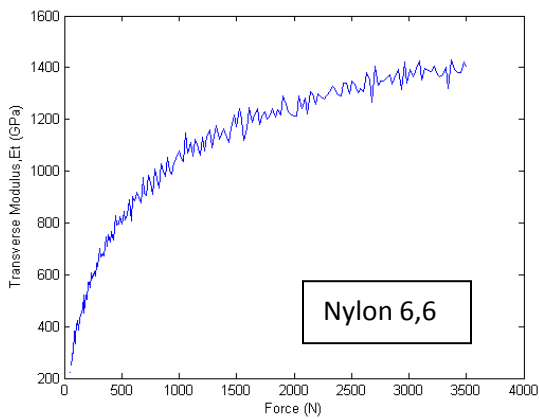
(a)
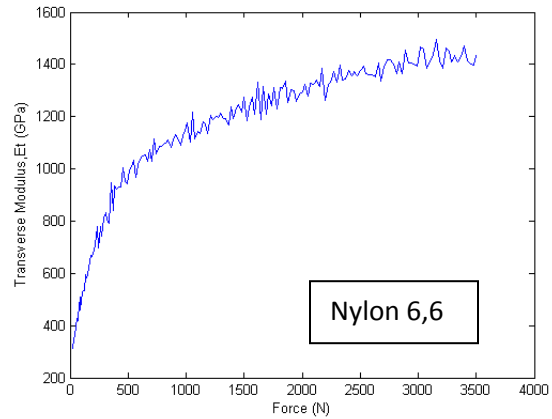
(b)
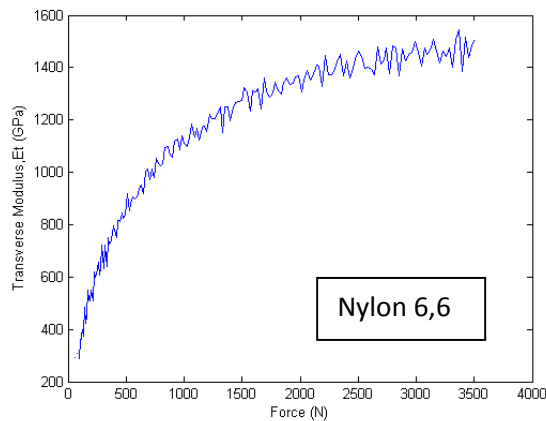
(c)

Figure 15: Graph of Transverse modulus, E_T Vs Force for four specimens tested

3 samples were tested and maximum transverse modulus was noted. It was observed that with the increase in force, the slope of the graph of transverse modulus Vs force decreased gradually

and thus the values of transverse modulus became more and more stable as the force increased.

Table 5: Maximum transverse modulus for Nylon 6,6 rods

Specimen number	$E_{T(max)}$ (GPa)
1	1.49
2	1.53
3	1.59
Average	1.54

An average modulus of 1.54 GPa was obtained, as shown in Table 3. The published value of transverse modulus found was 1.6 GPa. The value found experimentally and the published value was found to be close and thus this proved the credibility of our setup, method and procedure.

Results

A graph of E_T Vs force, was plotted for the all the samples tested. Figure 15 shows representative graphs of each yarn tested.
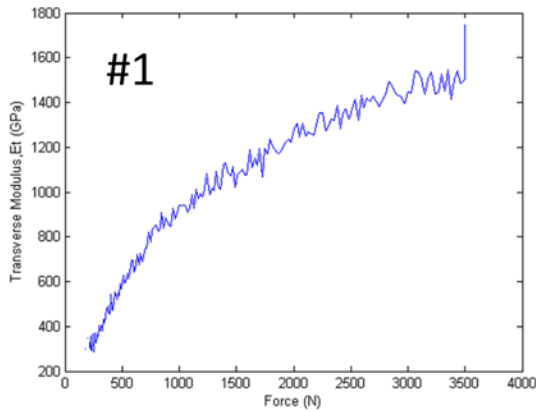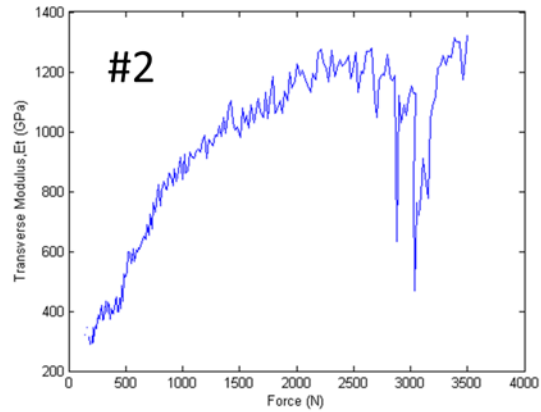
(a)   (b)
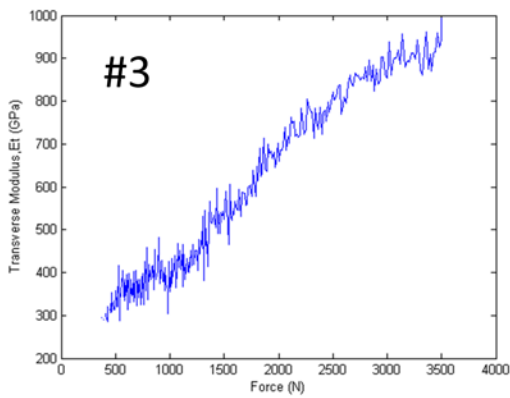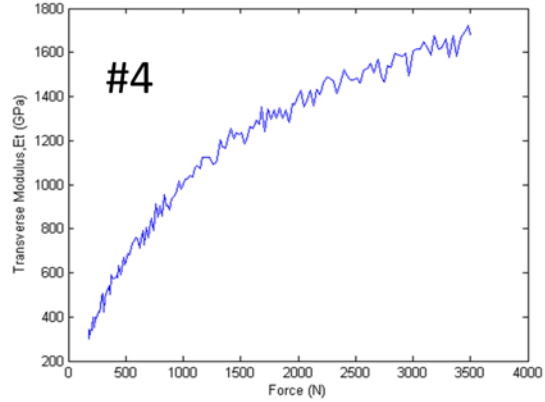
(c)   (d)

Figure 16: (a), (b),(c),(d) shows E_T Vs Time for one specimen each of yarn #1, #2, #3, #4

Linearly increasing values of E_T were obtained. This was because of the yarn made of several thousand filaments of prepreg carbon fiber and textile fiber. The braided yarn is not a filament by itself (for which the Hertzian-contact model is defined) but a bundle of several different fibers. During the application of load, as the yarn cross section is compressed, the packing density of the fibers of the cross section increases and this causes the yarn to stiffen progressively with the increase in load and thus time.

Now, all the test specimens were loaded to 3500 N during the course of test. Thus E_T at the same load would be comparable to find the yarn that performed the best in these tests. Thus, it was decided that $E_{T(max)}$ would be considered as the value which of transverse modulus to compare the performance of each yarn. Table 3 shows the results for $E_{T(max)}$ all the 4 types of yarns tested.

Table 6: $E_{T(max)}$ for yarn #1, #2,#3,#4

Type of yarn / Sample number	E_t for #1 (GPa)	E_t for #2 (GPa)	E_t for #3 (GPa)	E_t for #4 (GPa)
1	1.88	1.87	1.10	1.86
2	1.85	1.37	1.10	1.67
3	1.6	1.44	1.06	1.62
4	1.57	1.33	1.14	1.57
5	1.87	1.42	1.33	-
Average $E_{t(max)}$	1.75	1.49	1.15	1.68

Standard Deviation	0.155	0.218	0.106	0.126

Conclusion

The values of $E_{T(max)}$ found for yarns #1,#2,#3 and #4 are in the range of 1 to 2 GPa. The values are found to be relatively close with the difference between the maximum and minimum being 600 MPa. This is because of all the yarns having the same core. The approximate diameter of the core in all the 4 types of yarns is 1.8 to 2 mm. The fibers in the jacket account for the rest of the diameter. The undulation of the helical and the axial fibers in the jacket does not affect accuracy of the calculation of E_T to a large extent. Though no published data has been found that reports on the transverse modulus of prepreg composite carbon fiber yarns of circular cross, the value of E_T obtained for the yarns is similar to that found for Kevlar^{TM} KM2 fibers which have E_t of 1.34 GPa [13].

Transverse modulus of the yarn is an important property for the hoop strength of the O-ACS tubes. These tubes are not currently being used in applications where hoop strength of the tubes is important (example: O-ACS tubes used to make pressure vessels). The increasing nature of the transverse modulus is because of the increase in packing density of the yarn while being compressed. This means improving the packing density could improve the transverse modulus of the yarn. However, it should be noted that excessive increase in packing density could cause fiber breakage.

Flexural Modulus

Introduction

Flexural modulus of the yarns can be found by various tests. The most widely used techniques involve the 3 point bend test, the 4 point bend tests. The ASTM standards and guidelines were followed for performing these tests. Though it was found ASTM D790 [8], Flexural properties for reinforced plastics describes the procedure, calculations and guidelines for the test setup for laminate composites. Braided yarn is circular in cross section and thus the calculations for the stress and cross section area varied from the prescribed by the ASTM standards.

As prescribed by the ASTM standard D 790 the length to depth (l/d) ratio in the beams for a 3 point bend test should be above 16:1 [8]. These dimensional details make sure that there is negligible amount of shear deformations at the point of loading. Length to depth ratio lesser then 16:1 leads to stiffening of the beam and thus over estimates the flexural modulus.

Test Setup

Braided yarns of 4 kinds of different architectures were tested [Table 1]. Yarns of length 8 inches were used for the test. Span length for all the samples was kept to 6 inches with 1 inch over hang on the either side. All tests were performed on Instron^{TM} 5565 using a 3 point bend fixture as shown in Figure 16.The load and displacement data was extracted for all the tests from the Instron^{TM} machine and this data was further used to generate the Stress Vs Strain curves for the samples.
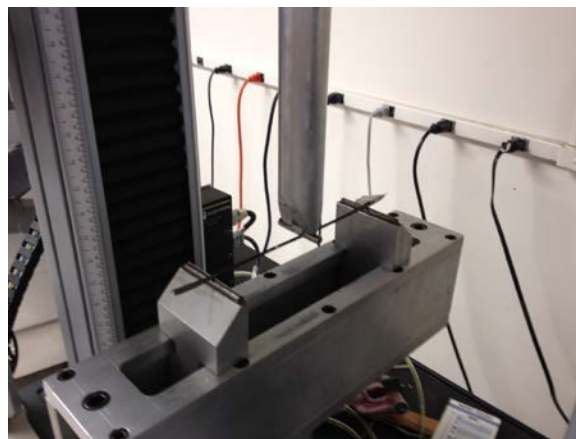
Figure 17: 3 point bend fixture for flexural modulus

Results

From the load and displacement data the stress and strain were calculated at all the points using the formulae [9,10] shown below:

Stress, σ = $\dfrac{FL}{\pi r^3}$ Equation 11

Strain, ϵ = $\dfrac{6Dd}{L^2}$ Equation 12

Here F is the force, L is the span length, r is the radius, and D is the deflection of the center point and d is the diameter

7 samples of each type of yarn were tested. Figure 17 show the Stress Vs Strain graphs for yarn #1, #2, #3, #4.
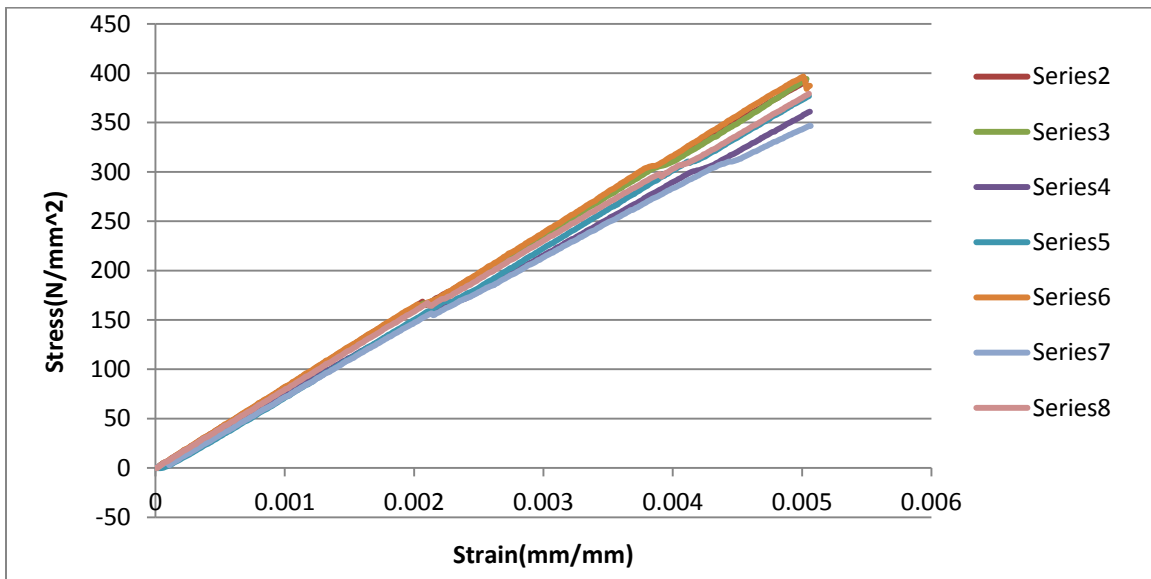
(a)
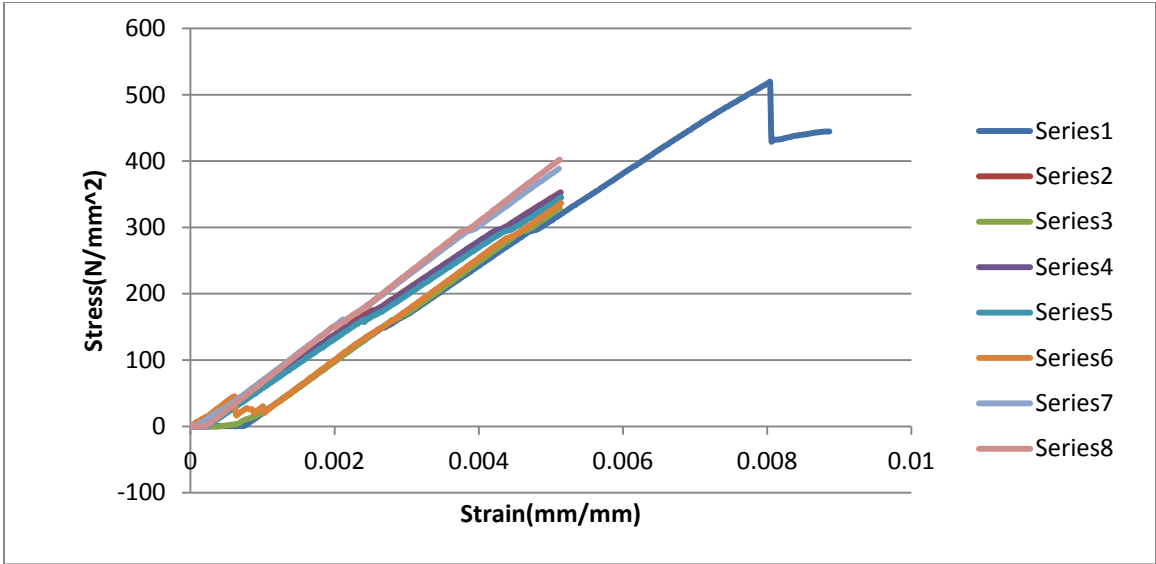
(b)
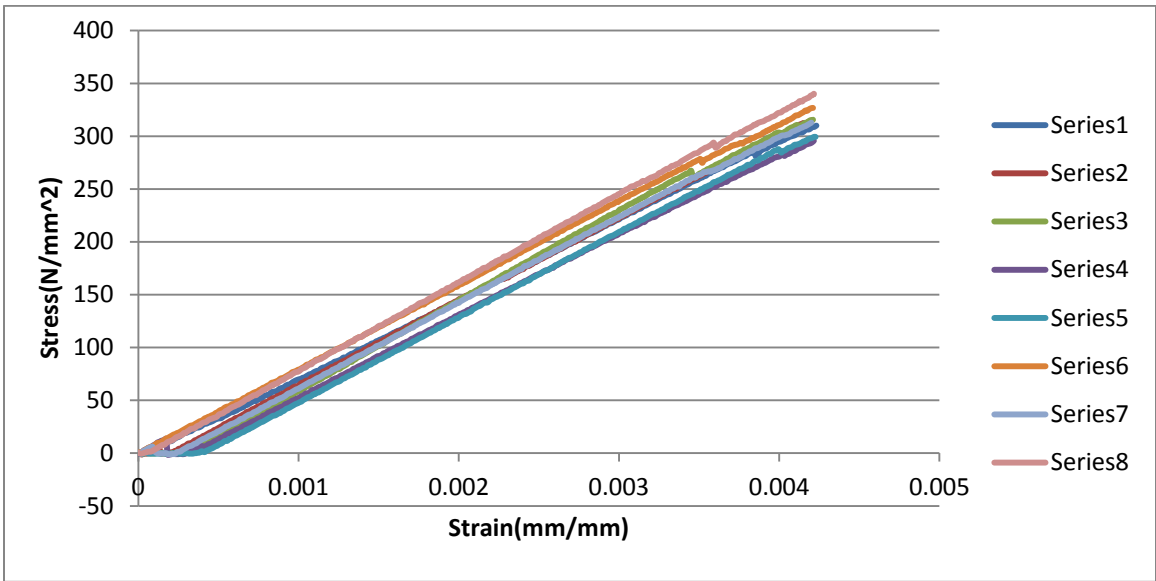
(c)
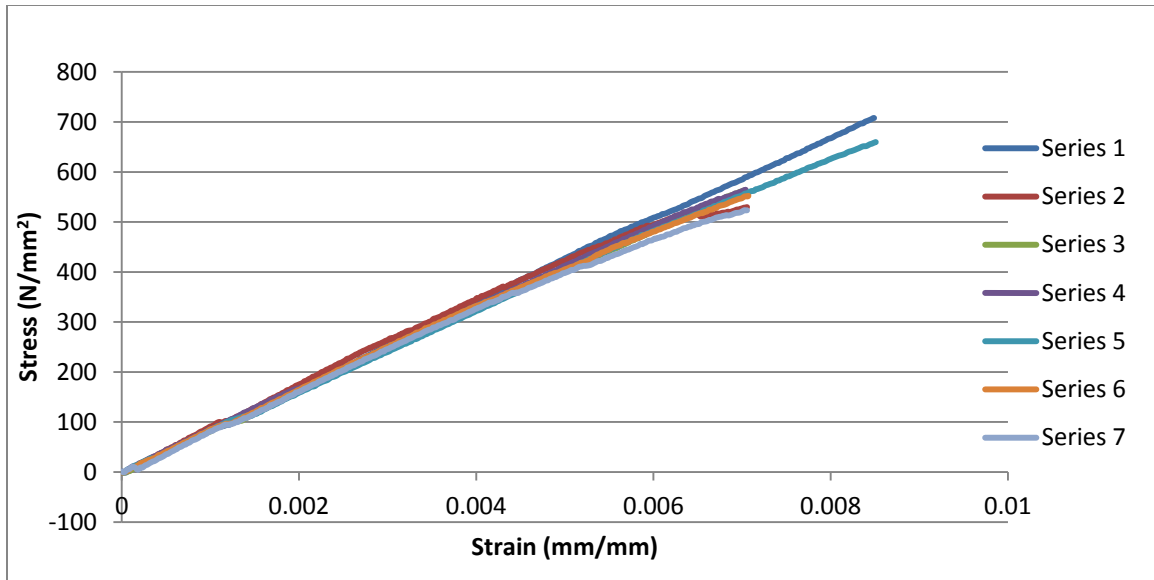
(d)

Figure 18 : (a),(b),(c),(d) Stress Vs strain graph for #1, #2, #4, #3

Table 4 shows the value of flexural modulus obtained and Figure 18 shows the comparison of the flexural moduli for the different yarns tested.

Table 7: Flexural modulus values for yarns

Type of yarn / Sample No	#1 (GPa)	#2(GPa)	#3 (GPa)	#4(GPa)
1	74.510	69.95	84.25	78.66
2	72.803	74.79	79.34	81.74
3	68.157	70.29	80.79	76.02
4	69.314	68.96	81.04	79.51
5	75.151	75.92	78.56	77.96
6	66.476	77.40	79.34	79.44
7	72.386	80.98	76.84	81.97
Average Flexural modulus	71.257	72.44	80.02	78.86

Standard Deviation	3.307	4.474	2.334	2.085
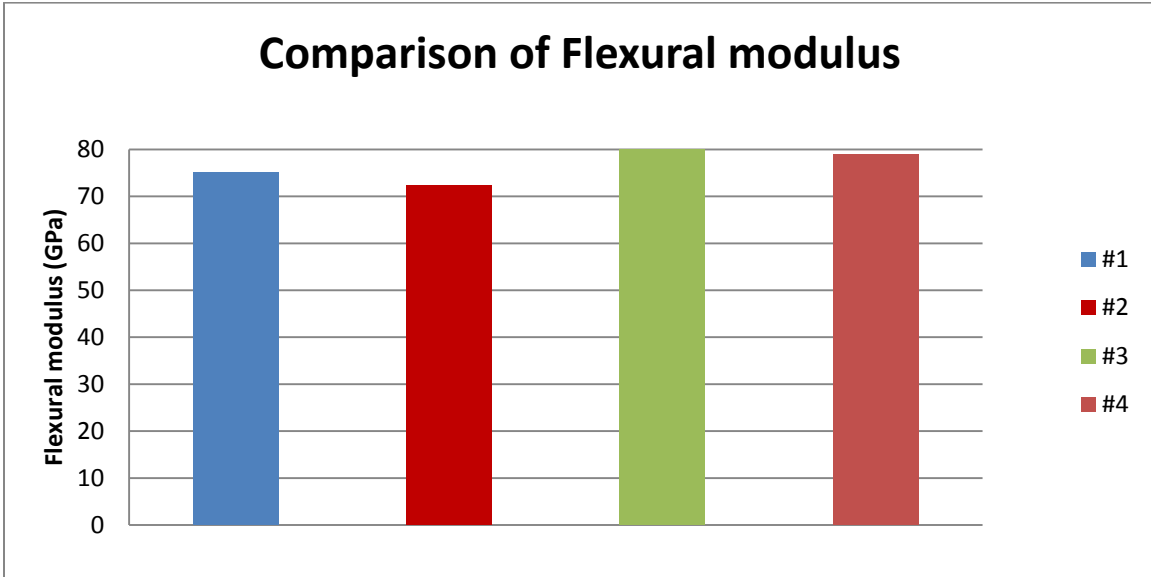
Figure 19: Graph comparing flexural modulus for yarns #1,#2,#3 and #4

Conclusion

From the results it is seen that the flexural modulus remains nearly the same for the yarns tested. This is because all the 3 different types of yarns tested have the same core ,that is, 48K T700 prepreg tows. Though the yarn #1 and #2 have excess prepreg carbon tow and dry carbon tow in the jacket relative the jacket of yarn #4 , their flexural modulus was not found to be higher than that of yarn #2.

References

1. S. L. PHOENIX and J. SKELTON, *Textile Res. J*. **65** (1974) 934

2. S. KAWABATA, *J. Textile Inst*. **81** (1990) 433

3. S. A. JAWAD and I. M. WARD, *J. Mater. Sci*. **13** (1978) 1381

4. Bourgoyne and Brown , Transverse properties of bulk aramid fibres, Standalone Document

5. Romain Maurine, Peter Davies, Nicolas Baral and Christophe Baley, *Applied Composite Materials*, March 2008, Volume15, Number 2:pages 61-73

6. J. Singletary, H. Davis, *Journal of Material Science* 35 (2000) 573-581

7. J. Singletary, H. Davis, *Journal of Material Science* 35 (2000) 583-592

8. ASTM Standard D-790-84a, Test Methods for flexural properties of unreinforced and reinforced plastics and electrical insulating materials

9. R. C. Hibbeler, Mechanics of Materials, Seventh edition, Chapter 6,pg 303

10. Three point bending formulae, http://en.wikipedia.org/wiki/Three_point_flexural_test

11. MATLAB^TM Help file ,*fzero*

12. S. B. WARNER, "Fiber Science" (Prentice Hall, Englewood Cliffs, NJ, 1995)

13. Subramani Sockalingam, John W. Gillespie Jr., Michael Keefe, On the transverse compression response of Kevlar KM2 using fiber-level finite element model, *International Journal of Solids and Structures*, Available online 26 March 2014, ISSN 0020-7683

Chapter 4 Poisson's Ratio

Introduction

Strain under load as well and the Poisons ratio is critical to the understanding of mechanical properties of materials, but is often difficult to measure. In composites, we should know these properties for both the textile reinforcing material, and the finished composite. The attachment of strain gages or a one dimensional (line) camera have proved useful in determining strain in one direction, typically the test direction in tensile testing of materials. Beginning in the early 1980's, a photographic/video technique known as Digital Image Correlation, or DIC, has been available to measure the deformation in two dimensions simultaneously. We have developed a system using off the shelf hardware components and freeware subroutines in MATLAB^{TM} to accomplish DIC measurements for strain and Poisons ratio on carbon epoxy composites. This effort is illustrated by application of DIC to a carbon fiber reinforced composite material during a tensile test. The difficulties encountered and the results of our testing are reported.

Open architecture composite tubes made by braiding prepreg Carbon Fiber Reinforced Polymer (CFRP) have a high strength/stiffness to weight ratio and thus might be used extensively in minimal weight applications. Much work has been done on the manufacturing process [9, 11], citing its potential in minimal weight applications [12] and design possibilities [10] in the past few years. For the development of these tubes from the minimal weight applications to a broader application where they are being used as structural reinforcement members for architectural structures, it is important to understand the building block of these tubes and that is the composite yarn, from which the tubes are constructed via braiding.

This composite yarn is made of pre-impregnated CFRP tow in the core and a textile yarn as a braided jacket. This structure not only gives the yarn reasonable braid ability but importantly, also gives the CFRP tow geometric stiffness. A good understanding of this marriage requires us to know all the intrinsic mechanical properties of the resultant yarn. Currently, work is being done on finding the modulus of elasticity and shear modulus along the three axes of the composite yarn. This paper represents our work done in finding the Poisson's ratio of the yarn along the local *x* and *y* axes as shown in the Figure 19
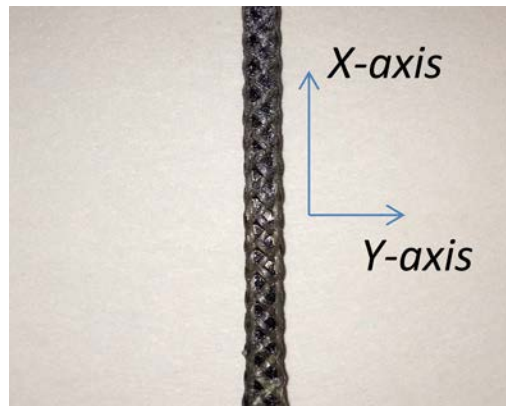
Figure 20: Braided yarn with local *x* and *y* axes, 2.03mm diameter before loading

There are several techniques that have been used to find Poisson's ratio for different kinds of materials and geometries. Usage of strain gauges to find Poisson's ratio [13] has been the most popular technique. Researchers have also used nondestructive techniques like X-ray methods [4] for thin films, beta-ray absorption methods [1] for rubber tapes, impact echo methods for solid circular rods [2], extensometers and strain gauges for studying fatigue in composites by monitoring Poisson's ratio [5] . One shortcoming in these non-destructive methods and usage of extensometers is that they are either or low precision and accuracy, or are extremely expensive for the initial setup. A new in-expensive technique, 2D digital image correlation, which has been used extensively in the past for full field measurements, has been used for finding Poisson's ratio in this study.

While the implementation of 2D DIC with high end cameras and commercially available software codes can be prohibitively costly, we have used an open source MATLAB^{TM} code jointly developed by researchers in John Hopkins University and Karlsruhe Institute of

Technology (KIT), Karlsruhe, Germany [14]. We have used a stereo microscope and a 10MP CMOS array digital camera for the microscope to record data.

Usage of 2D DIC for a yarn having circular cross section poses several challenges pertaining to correlation of the subsets, accuracy of the strain data, and size of the speckles. Our approach in overcoming these challenges has been discussed in this paper in the later sections.

Principal of 2D Digital Image Correlation

Since 1980s, several optical methods for finding the state of stress and strain over an entire field of view of the test specimen have been developed. Digital Image correlation is a white light non interferometric method that is capable of giving full field measurements. This has advantages over strain gauges which can only detect strains; only in the region they are attached. In DIC, images are recorded at the time of load application and then the each image is compared to the base image by matching a set of pixels in the subsequent image to the same set of pixels in the base image. The area of interest over which the displacements are to be tracked is covered with speckle pattern spray painted or applied with a brush. Each pixel in the image on which the speckle pattern is applied now has a unique gray scale intensity which is unique and unlike any other pixel in the image. The DIC code employs a correlation algorithm that correlates a set of pixels with certain grayscale intensity to the same set of pixels in the base image. Correlation algorithms are used for this purpose. The gray scale intensities change abruptly from pixel to pixel in an image and this can cause difficulties in the process of correlation. This is overcome by smoothing the intensities over the full image using different kinds of smoothing functions like bi-linear interpolation, bi-cubic interpolation, bi-cubic spline interpolation [15]. The displacement data obtained in terms of pixels can be differentiated to get the strains and stresses.

Test Vehicle and Experimental Setup

The yarn, used for the test is made of made of two components, a unidirectional prepreg carbon core and a braided jacket. The core is made of 4 X 12K prepreg carbon fiber tows, pulled and collected together. The core is the major contributor to the axial stiffness of the yarn. The jacket is made of Vectran[TM] or the conventional fibers braided around the core to hold the core tows together during subsequent formation by braiding of open truss composite structures [9]. This braided jacket consolidates the core fibers efficiently, protects them during the braiding processes and minimizes problematic residue transferred to the machinery.

The yarn used for the current experiment is made of four 12K CFRP tows. This resulted in a 48K CFRP unidirectional core. The jacket consists of a true tri-axial braid made of Vectran[TM] fiber. Since the axial fibers in the true tri-axial braid interweave with the helical fibers, the resulting braid is found to be very stable. The true tri-axial braid of Vectran[TM] fibers is made of 4 axial axial yarns and 8 helical yarns, 4 of which are clock wise and 4 anticlockwise.

The resulting yarn is approximately 2mm in diameter Figure 20. Since the jacket is braided, it does not have smooth outer surfaces. Because of the open lattice construction of the jacket, the diameter of the yarn changes along the periphery of the cross section and along the length.
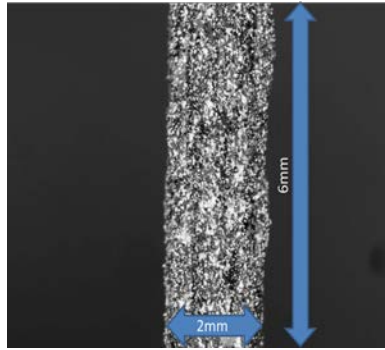
Figure 21: Braided yarn with dimensions

A 2D DIC setup consists of a recording device and a software code to perform the correlation work. The recording device is often a DSLR camera with a CCD array. The selection of the recording device is based on two parameters, the nature of loading and the size of the object. For our purpose, a stereo microscope equipped with a 10 MP CMOS array microscope camera inserted in 1 eye piece tube, has been used. The braided composite yarn is 2mm in diameter and thus needs to be magnified to get good resolution. Thus it would have been almost impossible to get the speckle pattern in focus with anything apart from a microscope which could zoom in on a 5 mm by 2 mm area at the center of the yarn. An open source 2D DIC MATLAB[TM] code has been used for the study. This MATLAB[TM] code uses a normalized cross correlation algorithm for correlation.

$$\sum \gamma(u,v) = \frac{\sum_{(x,y)}(x,y)[f(x,y)-\acute{f}(u,v)][t(x-u,y-v)-\acute{t}]}{\{\sum_{(x,y)}[f(x,y)-\acute{f}_{(u,v)}]^2 \sum_{(x,y)}[t(x-u,y-v)-\acute{t}]^2\}^{0.5}}$$

Equation 13

Here, in Equation 13, f is the image, t is the template of the pattern of size N_x and N_y, $\bar{t}$ is the mean of the template, u and v are x and y displacement of a pixel , $f(x,y)$ is the intensity value of image f of size M_x and M_y at point (x,y) in the image, $\bar{f}_{(u,v)}$ is the mean of $f(x,y)$ in the region under the template, γ is the normalized correlation value. $\gamma(u,v)$ is the normalized cross correlation value which is calculated at each point (u,v) to find the instantaneous position of the pattern, t in the image f [18]. Using the algorithm the position of the displaced pattern is found in the subsequent images.

The braided composite yarns of length 30 mm were coated with black and white spray paints with matte finish. As the field of vision was small, the speckle size had to be kept small to aid the correlation process.To achieve a small speckle size, each spray cannister used for applying the speckle pattern would be used only for 5-7 sprays. This is done because as the pressure within the spray cannisters drops the aerosol particles come together forming particles of bigger size. The yarn with the speckle pattern was then mounted on the UTM (Instron[TM] 5565) and a preload of 200 N was applied. The application of pre-load was to cancel out the rigid body movement of the yarn caused by the UTM once it starts applying the load on the sample. The inclusion of the rigid body displacement would directly affect the strain data.

The microscope with the camera was mounted on a fixture with a tripod as shown in the schematic in Figure 21. To achieve symmetric lighting, a LED ring light was mounted on the microscope. As a tensile load was applied on the yarn ,a video of the test specimen was recorded. This video was then converted into frames. These frames were then processed by the MATLAB[TM] code.
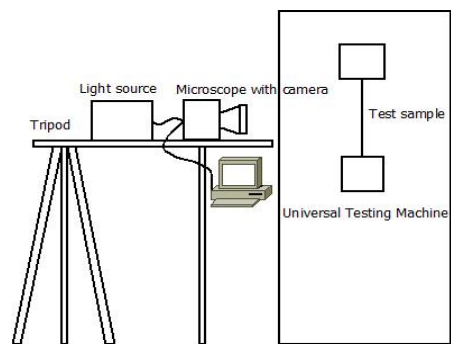
Figure 22: Schematic of the experimental setup

The resolution of the microscope camera is 1792x1374 pixels. To ensure good correlation, its is mandatory to ensure that the individual speckles are big enough to cover the full subset and is not so small as enough to remain entirely within a single pixel [15,6]. This can also be controlled by controlling the subset size [7]. A subset size of 15x15 pixels was found to be good for correletion after observing several speckles in different yarns at the magnification where the image was pixelated as hown in Figure 22. The least count of the system was found to be 0.54 pixels by processing the images of the specimen,obtained , while no load was applied for a short duration of time.
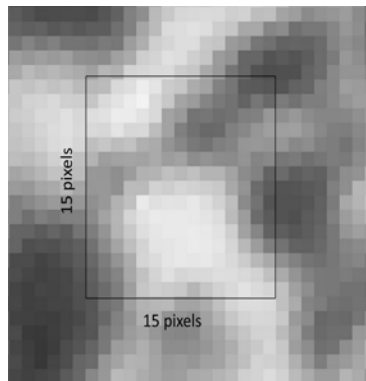
Figure 23: Pixilated view of the speckle pattern , showing the subset size

Calculation of Poisson's Ratio

DIC is a full field measurement technique that is popular for giving displacements and its derivatives as contour plots that lets the researcher analyze the stress-strain distribution [16], regions of stress concentration [8],stress intensities around a crack tip [17] and several other applications. Two dimensional (2D) DIC has also been used by researchers to obtain mechancial properties like modulus of elasticity and shear modulus [3]. Literature review showed that not much work has been done in successfully finding the Poisson's ratio. Poisson's ratio being the ratio of lateral to longitudinal strain has an inherent difficulty that the amount of strain induced in the sample is very small as the load on the sample is always kept within the material's elastic limit. This makes visual detection of visual strain challenging.Though DIC technique is capable of giving subpixel accuracy, there are several means through which error can be induced easily. Separating the rigid body motion from the true displacement is difficult because of difficulties in correlation of the markers due to improper subset size,fading of white speckles due to improper lighting, plane of the camera and the plane of the sample not being parallel. These sources of

44

error induce errors in displacements and thus the strain values required for the Poisson's ratio are affected.

An additional difficulty in our attemp at finding the Poisson's ratio was using a 2D DIC technique on a yarn with a circular cross section. The attempt was made on the premise that the yarn was circular in cross section and thus being able to detect the radial strains on the periphery would give a true indication of the lateral strains. This meant that being able to view the periphery to detect the radial strain was of paramount importance. This was achieved succesfully by using a stereo microscope fitted with a camera. But usage of microscope also posed the challenge of producing a small enough speckle size.

The tensile test on the yarn was captured recorded in the form of video and then converted into frames. All the DIC codes commercially available let the user define a Region Of Interest(ROI) over the which a grid of markers would be placed. These markers are the centers of the subsets in the region of interest.The MATLAB^{TM} code that we used allowed the user to define the region of interest in several ways. Since the ROI in our experiment was on the periphery, a line of markers was defined on both the right and the left boundaries of the yarn. Since the region visible to the microscope was circular in cross section it was important to define the markers as close to the periphery as possibleas shown in Figure 23. The circular profile of the yarn would be perceived as a geometry of a planar rectangle through the microscope. This meant that the radial strain detected would be true only at the boundaries and the strain values would diminish relative to the true strain values as we go towards the center of the planar rectangle.
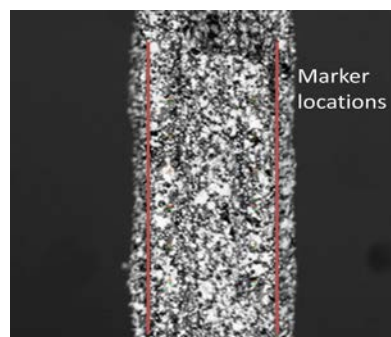
Figure 24: Braided yarn with the marker locations

The data was obtained from the 2D DIC MATLAB code in the form of true strain along local x and y axis. These strain values were then used to obtain the Poisson's ratio by plugging them in equation below.

$$Poisson's\ ratio, v = \frac{true\ strain\ along\ local\ y\ axis}{true\ strain\ along\ local\ x\ axis} \qquad \text{Equation 14}$$

The true strain was obtained for every frame and thus for each test piece , Poisson's ratio was obtained for each frame correlated. The Figure 26 shows an example of the true strains obtained. From the example graph which is representive of the form in which all the data was obtained , it was seen that ratio of the value at a peak on the graph with the corresponding valley in the same frame number would induce noise in the calculation of the average Poisson's ratio. To filter out this noise, a running average of 4 data points were calculated. This process ensured that the magnitude of the error was minimized.

Method Verification

Before starting to test the braided composite yarn, it was of important to the verify the accuracy of the results obtained from the test fixture made, the DIC MATLAB^TM code and approach selected for calculating the Poisson's ratio. It was decided that the Poisson's ratio of a metal would be found and compared to its known value. This would give a right estimate of the accuracy of setup, MATLAB^TM code and the approach. Strips of aluminum 6061 T6 were were used for this pupose. This aluminum alloy is known to have Poisson's ratio of 0.33. Aluminum strips of dimension 14"x1.5"x0.1" were used for the test. Figure 24 show the speckle pattern on the aluminum test pieces and the Gaussian distribution of light intensity over the test piece. This Gaussian distribution of the grey scale intensities meant that the lighting over the full field of the specimen was symetric.
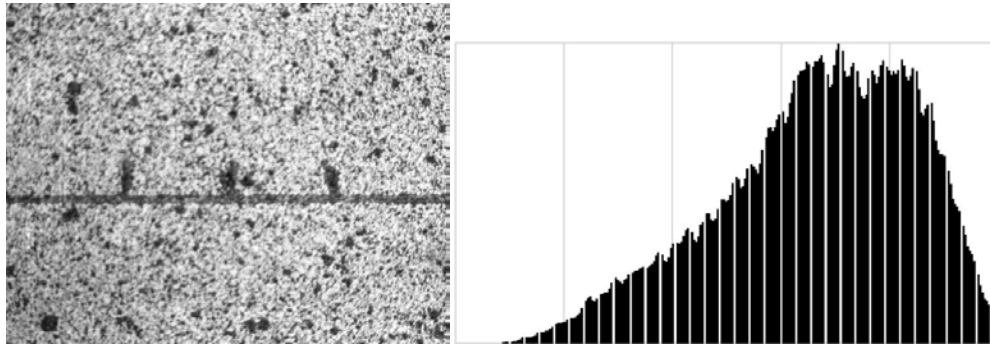
Figure 25: (a) Speckle pattern on the AL test piece, (b) Histogram of the gray scale intensities

Three samples of the AL 6061 T6 were tested. The results were obtained from the graphs of Poisson's ratio Vs Image number as shown in Figure 25, following the same procedure mentioned earlier. Table 5 shows the Poisson's ratio for the three samples.
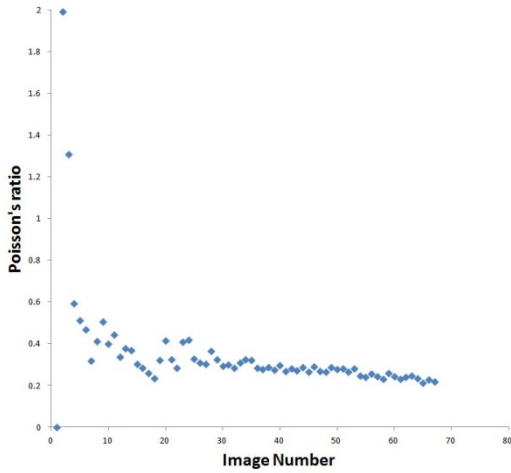
(a)
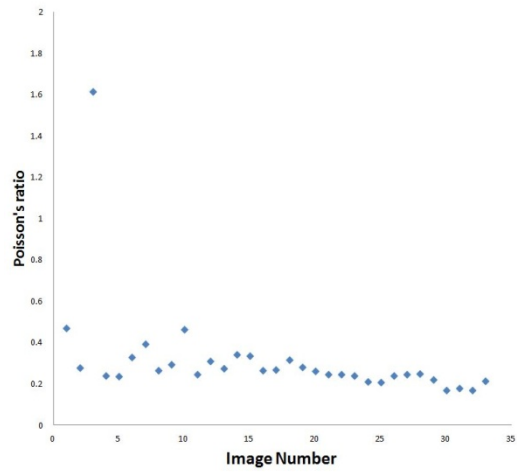
(b)
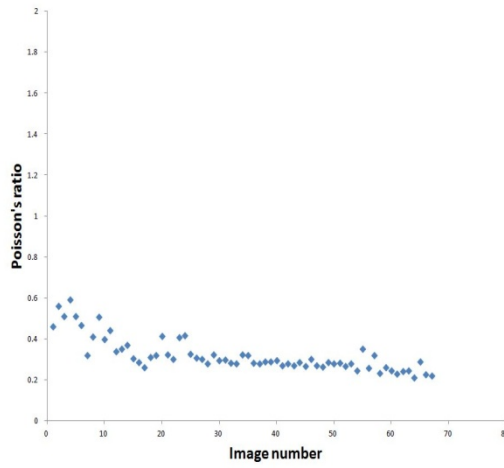
(c)

Figure 26:(a),(b) and (c) : graph of Image number Vs Poisson's ratio for Test piece 1,2,3

Table 8: Poisson's ratio for AL 6061 T6 test pieces

	Poisson's Ratio	% error in comparison to the known value
Test piece 1	0.3087	6.45
Test piece 2	0.3123	5.36
Test piece 3	0.3210	2.73

It was seen in that the Poisson's ratio obtained for the samples were within 7% error in comparison to the known Poisson's ratio of 0.33 of AL 6061 T6 alloy.

Results

After validation of the setup and the approach, tests were performed on the braided composite yarn as per the procedure mentioned earlier. Figure 26 shows the graph of true strain along *x* & *y* Vs image number and Figure 27 shows the graph of Poisson's ratio Vs Image number without taking the running averages.
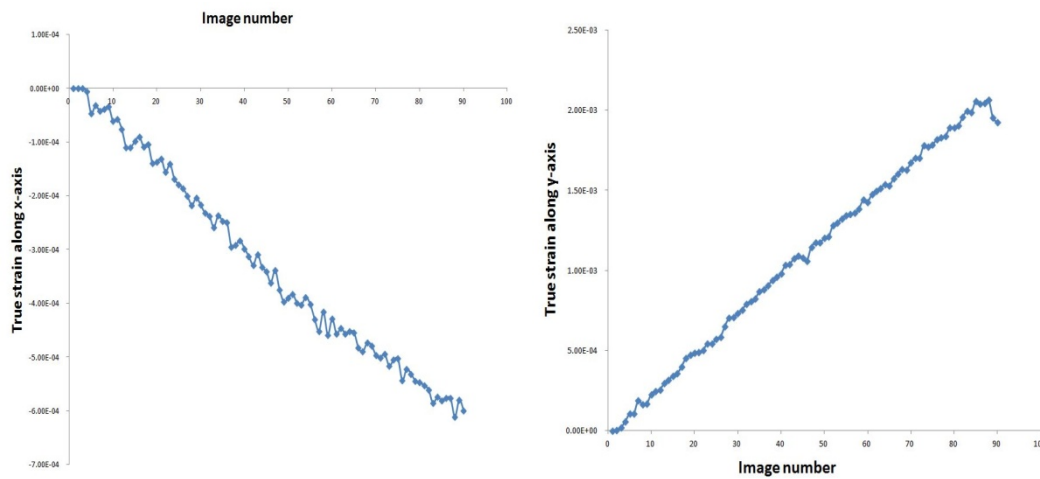
Figure 27: (a)True strains along *x* axis , (b)True strain along *y* axis
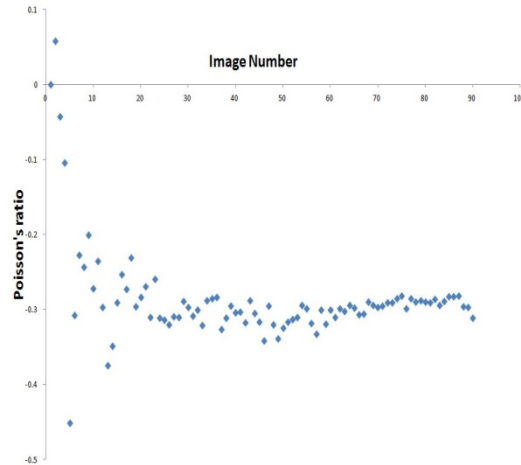
Figure 28: Poisson's ratio Vs Image number for test piece 1 without taking a running average

As seen from the graphs in Figure 26**,** a fairly linear nature of the strains was obtained for all the yarns tested, since the yarns were maintained within the elastic limit. The scatter plot of the Poissons's ratio against the image number is shown. This data was plotted without taking the running averages. It can be seen that there is considerable scatter at the beginning. This was because of the initial rigid body displacements in the yarn when the UTM started applying a tensile load. This scatter was present in the initial 10% of the frames and thus it was important to minimize the error induced by taking the running averages over small intervals. Graphs in

Figure 28 shows the graphs of Poisson's ratio Vs Image number of 5 test pieces of yarn #4.

(a)   (b)

50
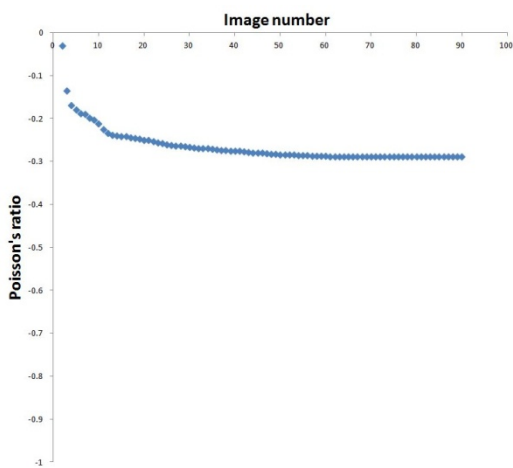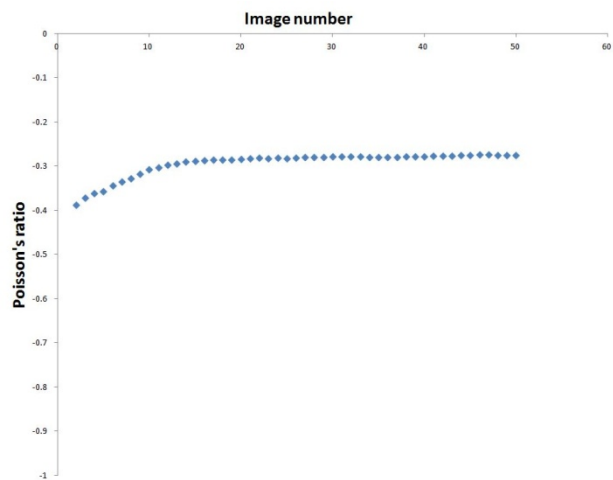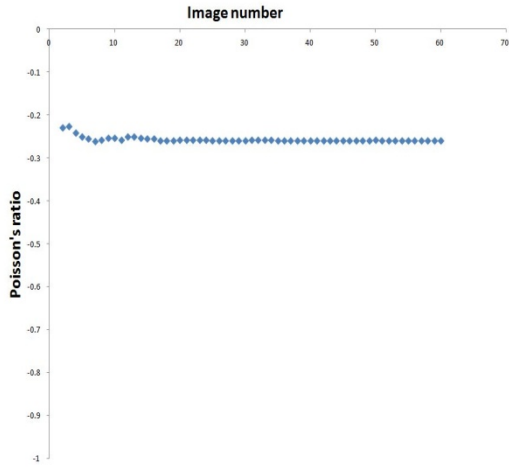
(c)
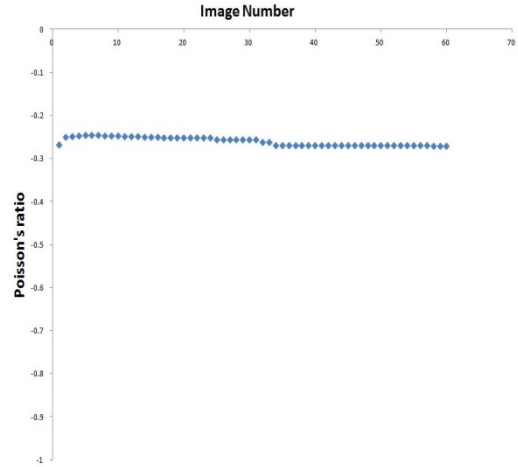
(d)
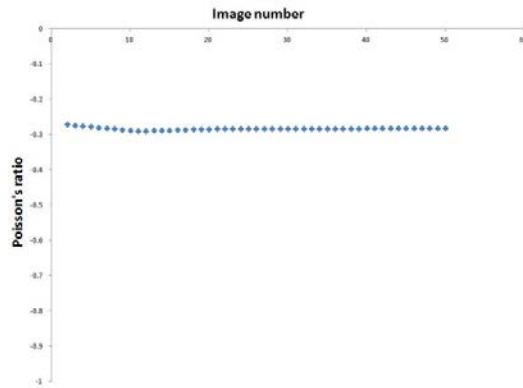
(e)

Figure 29: (a),(b),(c),(d) and (e) ,Image number Vs Poisson's ratio for samples 1,2,3,4 and 5

Table 9: Poisson's ratio for braided yarn

	Poisson's Ratio
Test piece 1	0.2646
Test piece 2	0.2934
Test piece 3	0.2565
Test piece 4	0.2596
Test piece 5	0.2838

From the data in Table 6 it is was clear that the Poisson's ratio was in the range of 0.2646 to 0.2934 for the five samples of the same make tested. The average Poisson's ratio was found to be 0.2716.

Conclusion

At the end of this study, considering the parameters used for 2D digital image correlation, speckle size, subset size, and non-perpendicularity of the yarn in the grips, were found to have direct impact on the amount of noise induced in the strain readings. The usage of a camera with a CMOS array instead of a CCD array and use of 2D DIC for a 3D yarn did affect the accuracy of the results obtained marginally. Now, all the 4 types of yarns made, had the same core ie 4 X 12K T700 prepreg tow and thus the value of Poisson's ratio found for yarn #4 would not change by a considerable amount. Thus, keeping in mind the accuracy of the system, the Poisson's ratio found for yarn #4 could be treated as a value common for other yarns with the same core size, ie yarn #1, #2 and #3.

The use of running averages to minimize the error caused by the initial rigid body motion was found to be only necessary for the braided yarn, circular in cross section and not the planar aluminum test pieces. This was because of the geometry and size of the braided yarn which was difficult to clamp firmly in the UTM's swivel grips. The approach taken to overcome these problems and the setup used for the entire study did yield decent accuracy. Considering this, the Poisson's ratio obtained for the braided composite yarn was found to be reliable for future work.

References

1. Jafar Fathi, Saleh Ashrafi, Hossein Movla, Samad Sobhaian, A novel method to determine Poisson's ratio by beta-ray absorption experiment, *Applied Radiation and Isotopes*, Volume 70, Issue 5, May 2012, Pages 823-826, ISSN 0969-8043

2. Jin-Jun Wang, Ta-Peng Chang, Bo-Tsun Chen, Helsin Wang, Determination of Poisson's ratio of solid circular rods by impact-echo method, *Journal of Sound and Vibration*, Volume 331, Issue 5, 27 February 2012, Pages 1059-1067, ISSN 0022-460X

3. F. Laurin, J.-S. Charrier, D. Lévêque, J.-F. Maire, A. Mavel, P. Nuñez, Determination of the Properties of Composite Materials Thanks to Digital Image Correlation Measurements, *Procedia IUTAM*, Volume 4, 2012, Pages 106-115, ISSN 2210-9838

4. Wei-En Fu, Yong-Qing Chang, Bo-Ching He, Chung-Lin Wu, Determination of Young's modulus and Poisson's ratio of thin films by X-ray methods, *Thin Solid Films*, Volume 544, 1 October 2013, Pages 201-205, ISSN 0040-6090

5. W. Van Paepegem, I. De Baere, E. Lamkanfi, J. Degrieck, Monitoring quasi-static and cyclic fatigue damage in fibre-reinforced plastics by Poisson's ratio evolution, *International Journal of Fatigue*, Volume 32, Issue 1, January 2010, Pages 184-196, ISSN 0142-1123

6. G. Crammond, S.W. Boyd, J.M. Dulieu-Barton, Speckle pattern quality assessment for digital image correlation, *Optics and Lasers in Engineering*, Volume 51, Issue 12, December 2013, Pages 1368-1378, ISSN 0143-8166

7. Sun Yaofeng, John H.L. Pang, Study of optimal subset size in digital image correlation of speckle pattern images, *Optics and Lasers in Engineering*, Volume 45, Issue 9, September 2007, Pages 967-974, ISSN 0143-8166

8. A.J. Comer, K.B. Katnam, W.F. Stanley, T.M. Young, Characterising the behaviour of composite single lap bonded joints using digital image correlation, *International Journal of Adhesion and Adhesives*, Volume 40, January 2013, Pages 215-223, ISSN 0143-7496

9. David John Branscomb*, Minimal weight composites using advanced manufacturing techniques, Doctoral Thesis*, Auburn University , 2012

10. D. Branscomb, A. Gurley, D. Beale, R. Broughton, "Open-Architecture Composite Tube Design and Manufacture" *ASME Early Career Technical Journal*, 2012

11. D. Branscomb, D. Beale, R. Broughton, "New Directions in Braiding", *Journal of Engineered Fibers and Fabrics*, volume 8, Issue 2-2013

12. D. Branscomb and D. Beale, "Fault detection in braiding utilizing low-cost USB machine vision*", The Journal of the Textile Institute*,Volume 102, Issue 7, 2011

13. D.J. Mead, R.J. Joannides, Measurement of the dynamic moduli and Poisson's ratios of a transversely isotropic fibre-reinforced plastic, *Composites*, Volume 22, Issue 1, January 1991, Pages 15-29, ISSN 0010-4361

14. Christopher Eberl,< http://www.mathworks.com/MATLABcentral/fileexchange/12413-digital-image-correlation-and-tracking> , 09/27/2006

15. Arun Shukla , James W. Dally, *Experimental Solid Mechanics*, Collegehousebooks,2013,1[st] Edition

16. Jakob Olofsson, Ingvar L. Svensson, Pascal Lava, Dimitri Debruyne, Characterisation and investigation of local variations in mechanical behaviour in cast aluminium using gradient solidification, Digital Image Correlation and finite element simulation, *Materials & Design*, Volume 56, April 2014, Pages 755-762, ISSN 0261-3069

17. Rui Zhang, Lingfeng He, Measurement of mixed-mode stress intensity factors using digital image correlation method, *Optics and Lasers in Engineering*, Volume 50, Issue 7, July 2012, Pages 1001-1007, ISSN 0143-8166

18. Briechle, Kai , Hanebech D. Uwe , Template matching using fast normalized cross correlation, *Optical Pattern Recognition XII*, 95 (March 20, 2001); doi:10.1117/12.421129

Chapter 5 Micromechanical modeling

Introduction

In the previous chapters we have discussed the development of various experimental techniques to find the mechanical properties of the yarn. Young's modulus along the axis (E_L), perpendicular to the axis (E_T), Poisson's ratio (ν_{LT}) and flexural modulus ($E_{flexural}$) were found experimentally. Often, it is found that experimentation can be time consuming and expensive in case of composite materials. This is because of the increase in the number of parameters required to fully define these non-homogenous, orthotropic materials [5]. For fiber –matrix composites, mathematical modeling of the physical properties of the composite has been comprehensively done in the past and it has been found to be reasonably accurate in comparison to the experimentation for certain physical properties [3]. In this chapter, considering the principles of weight fraction and volume fraction, an attempt has been made to develop a new micromechanical model specifically for the composite yarn.

The micromechanical modeling for the fiber-matrix composites is focused on unidirectional continuous fiber reinforced lamina [3]. A majority of the books on mechanics of composites materials have been found to have a section on the micromechanical modeling. The technique is very helpful to predict the mechanical properties of the composites before they are made. Micromechanical modeling is based on the premise that the physical properties of each of the constituents that form the composite contribute towards the aggregate properties of the composite [3]. The amount of contribution by each of the constituents is dependent on the volume, mass and density of the constituent. Researchers have extended the bases of these concepts to various applications like a model to predict the Young's modulus of adipose tissues [2]. Micromechanical models have been made for gauging damage in fiber composites [12].

Complex models for finding elastic properties of composites have been made [11]. Ultimate strength of composites and life prediction of transversely isotropic composites have been predicted using micromechanical models [6,7,8]. Researchers have found mechanical properties using computer simulations made by bridging two micro mechanical properties [9].Our work on developing a micromechanical model, especially to predict the mechanical properties of the yarn have been reported in this chapter.

The composite yarn resembles the laminae in a way that, the yarn is also predominantly made of the unidirectional long continuous prepreg carbon fiber. The textile fiber, for good braid ability and dry carbon fiber tow in the jacket, contributes to the axial stiffness and the torsional stiffness. The braiding of the jacket on to the prepreg T700 tow has also been found to increase the packing density of the resulting yarn. Depending on the architecture of yarn, the presence of textile fiber or high modulus fibers (like Kevlar[TM] fibers) and the carbon fiber tow in the jacket (if there) has been found to account for a minimum of 10% to a maximum of 35% of the weight of the yarn .Thus it is imperative that the effect of the fibers in the jacket cannot be neglected. Also the textile fibers in the jacket are at an angle arranged helically around the circumference of the yarn. The vertical component of the stiffness of fibers in the helix would contribute to the axial stiffness and the horizontal component would contribute towards the torsion stiffness of the yarn. To understand the effect of the fibers that make the jacket towards the overall behavior of the yarn and to accurately predict the properties of the yarn, it is important to modify the currently existing micromechanical model.

Existing Micromechanical Model

A short overview of the existing micromechanical model for laminates made the equations used are as follows is given below.
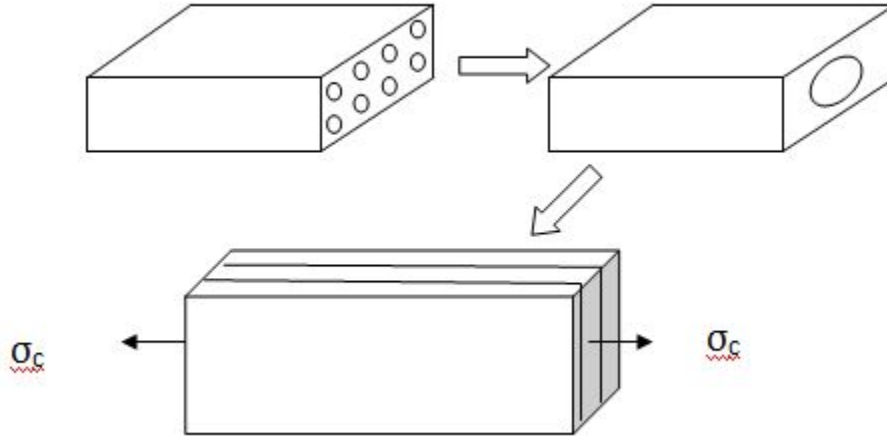
Figure 30: Volume element for the micromechanical model

Figure 29 shows the representative volume element for which the micromechanical model is made.

v_c, v_f, v_m = volume of composite, fiber, matrix respectively

P_c, P_f, P_m = density of composite, fiber, matrix respectively

The fiber volume fraction (V_f) and the matrix volume fraction (V_m) can be given as

$$V_f = \frac{v_f}{v_c}$$
Equation 15

$$V_m = \frac{v_m}{v_c}$$
Equation 16

The density of the composite is given as

Equation 17

$$P_c = P_f V_f + P_m V_m$$

The major Young's modulus is given as

$$E_l = E_f V_f + E_m V_m$$
Equation 18

The minor Young's modulus is given as

$$\frac{1}{E_t} = \frac{V_f}{E_f} + \frac{V_m}{E_m}$$

Equation 19

The major Poisson's ratio is given as

$$v_{c} = v_f V_f + v_m V_m$$

Equation 20

The major torsion modulus is given as

$$\frac{1}{G_{12}} = \frac{V_f}{G_f} + \frac{V_m}{G_m}$$

Equation 21

Figure 29 shows the representative unit cell of the laminate. This unit cell is assumed to remain the same for the composite yarn as well. These equations are meant for the lamina which is constituted by just the reinforcement fiber and the matrix. To further this model for a composite with more number of constituents, more terms have to be added that represents the textile fiber and the other fibers (if any) in the jacket.

Our initial literature review showed that transverse Young's modulus for circular fiber in rectangular unit cell is cannot be predicted accurately using micromechanical modeling developed from the mechanics of materials approach. The error in experimental values and the values obtained by micromechanical modeling increases with increase in fiber volume fraction [3]. Also E_2 for laminate is tensile modulus for weft fibers and E_2 for our yarn is the compressive modulus over the cross section of the yarn.

Modified Micromechanical Model

The modified micromechanical model is shown below. It is assumed to have the save representative unit cell.

v_c, v_{jh}, v_{ja}= volume of core, jacket helical fiber, jacket axial matrix respectively

P_c, P_{jh}, P_{ja}= density of core, jacket helical fiber, jacket axial matrix respectively

The core volume fraction (V_c), volume fraction of jacket helical fiber (V_{jh}) , volume fraction of jacket axial fiber(V_{ja}), volume fraction of second jacket axial fiber(V_{ja2}) can be given as

$$V_c = \frac{v_{core}}{v_c} \qquad\qquad \text{Equation 22}$$

$$V_{jh} = \frac{v_{jh}}{v_c} \qquad\qquad \text{Equation 23}$$

$$V_{ja} = \frac{v_{ja}}{v_c} \qquad\qquad \text{Equation 24}$$

$$V_{ja2} = \frac{v_{ja2}}{v_c} \qquad\qquad \text{Equation 25}$$

The density of the composite is given as

$$P_c = P_c V_c + P_{jh} V_{jh} + P_{ja} V_{ja} + P_{ja2} V_{ja2} \qquad\qquad \text{Equation 26}$$

The major Young's modulus is given as

$$E_c = E_c V_c + E_{jh} V_{jh} + E_{ja} V_{ja} + E_{ja2} V_{ja2} \qquad\qquad \text{Equation 27}$$

The minor Young's modulus is given as

$$\frac{1}{E_2} = \frac{V_c}{E_c} + \frac{V_{jh}}{E_{jh}} + \frac{V_{ja}}{E_{ja}} + \frac{V_{ja2}}{E_{ja2}} \qquad\qquad \text{Equation 28}$$

The major Poisson's ratio is given as

$$v_{12} = v_c V_c + v_{jh} V_{jh} + v_{ja} V_{ja} + v_{ja2} V_{ja2} \qquad\qquad \text{Equation 29}$$

The major torsion modulus is given as

$$\frac{1}{G_{12}} = \frac{V_c}{G_c} + \frac{V_{jh}}{G_{jh}} + \frac{V_{ja}}{G_{ja}} + \frac{V_{ja2}}{G_{ja2}} \qquad\qquad \text{Equation 30}$$

On basis of the modified model as shown above yarns of 4 different makes were analyzed. For this purpose, yarns of each type were cut to a known length and weighed on a weighing scale, accurate upto 4 decimal points. This gave the linear density in terms of milligrams/mm. Weight fractions for each constituent were found by separating each constituent in the yarn and weighing them separately. Densities of each type of fiber Table 7 were found and this data was used to find the volume fractions from weight fractions.

Sample calculations for yarn #2

Length of yarn cut = 30mm

Weight of the yarn, $W_{composite}$ = 0.20gms

Length of helical Kevlar^{TM} fiber = 36mm

Length of axial T700 core = 30mm

Length of axial yarns in the jacket = 32mm

Linear density of the constituent fibers was found by weighing 2 meter lengths of each fiber

Linear density of 3K T700 prepreg = 0.2545 gms/m

Linear density of 12K T700 prepreg = 1.075 gms/m

Core: 48K T700 prepreg tow (4 X 12K)

$W_c = w_c/W_{composite} = 0.645$

Jacket

8 X 400 denier Kevlar^{TM} fiber

$W_{jh} = w_{jh}/W_{composite} = 0.064$

4 X 3K T300 prepreg tow

$W_{ja} = w_{ja}/W_{composite} = 0.16288$

4 X 3K T300 dry carbon fiber tow

$W_{ja2} = w_{ja2}/W_{composite} = 0.1267$

Now, density of the composite yarn, $P_c = \dfrac{weight}{volume} = \dfrac{weight}{Area\ X\ Length} = \dfrac{0.20}{4.79\ X\ 3\ 0}$

$P_c = 1.39$ gm/cm^3

Table 10: Densities of fibers

Type of fiber	Density (gm/cm^3)
T700 tow	1.560
Kevlar^{TM}	1.440
T300 tow prepreg	1.539
T300 tow (dry)	1.760
Polyester	1.40
Nylon	1.30
Vectran^{TM}	1.40

Using the data in the Table 7 [4], volume fractions were found:

Core

$$W_c = \frac{P_c}{P_{core}} V_c$$

$V_c = 0.5747$ cm^3

Similarly the volume fractions of the fibers in the jacket were calculated and the results are reported below:

$V_{jh} = 0.06177$ cm^3

$V_{ja} = 0.14709$ cm^3

$V_{ja2} = 0.1$ cm^3

Using equations 31, 33 and 34 the Young's modulus, Poisson's ratio and torsion modulus were calculated.

Table 8 shows the results for yarn #2

Table 11: Mechanical properties for yarn #2

Property	E_L (GPa)	v_c	G_{LT} (GPa)
Yarn #2	120.253	0.1815	5.6589

Similar calculations for volume fractions were made using equations 26, 27, 28 and 29, for Yarn #1,#3, #4. Table 9 shows the results for volume fractions all the yarns

Table 12: Volume fractions fors yarns #1,#2,#3 and #4

Yarn type	V_{pcf}	V_{Tf}	$V_{pcf(2)}$	V_{dcf}
Yarn #1	0.5912	0.05809	0.1302	0.1159
Yarn #2	0.5747	0.06177	0.14709	0.1
Yarn #3	0.624	0.165	0.149	-
Yarn #4	0.91	0.0725	-	-

The material properties of composite core and the fibers in the jacket are reported in Table 10, [1], [4], [5]

Table 13: Various mechanical properties of fibers in the core and the jacket

Yarn type	E_L (GPa)	v_c	G_{LT} (GPa)
T700 (prepreg core)	135	0.2	5
Polyester	10.5	0.38	0.979
Kevlar^{TM}	70.5	0.36	5
Nylon	9.55	0.38	1.21
Vectran^{TM}	103	-	-
T300 dry	184.566	0.15	5

Results

Using the material properties in Table 10 and volume fractions from Table 9 , the engineering constants for the Yarn #1,#2,#3,#4 were found using equations 31,33,34

Table 14: Properties found using micromechanical model

Yarn Type	E_L (GPa)	v_c	G_{LT} (GPa)
#1	119.388	0.1837	4.409
#2	120.253	0.1815	5.658
#3	105.93	0.2173	2.037
#4	100.09	-	-

Conclusion
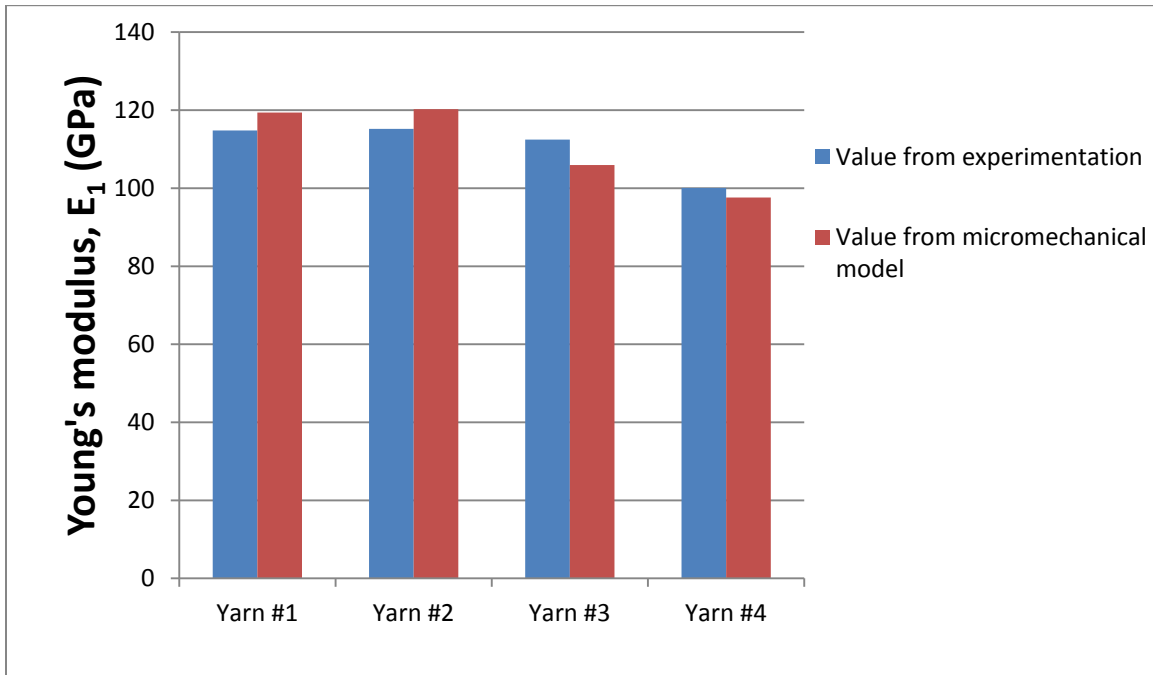
Figure 31: Comparison of E_L, found experimentally and using micromechanical model
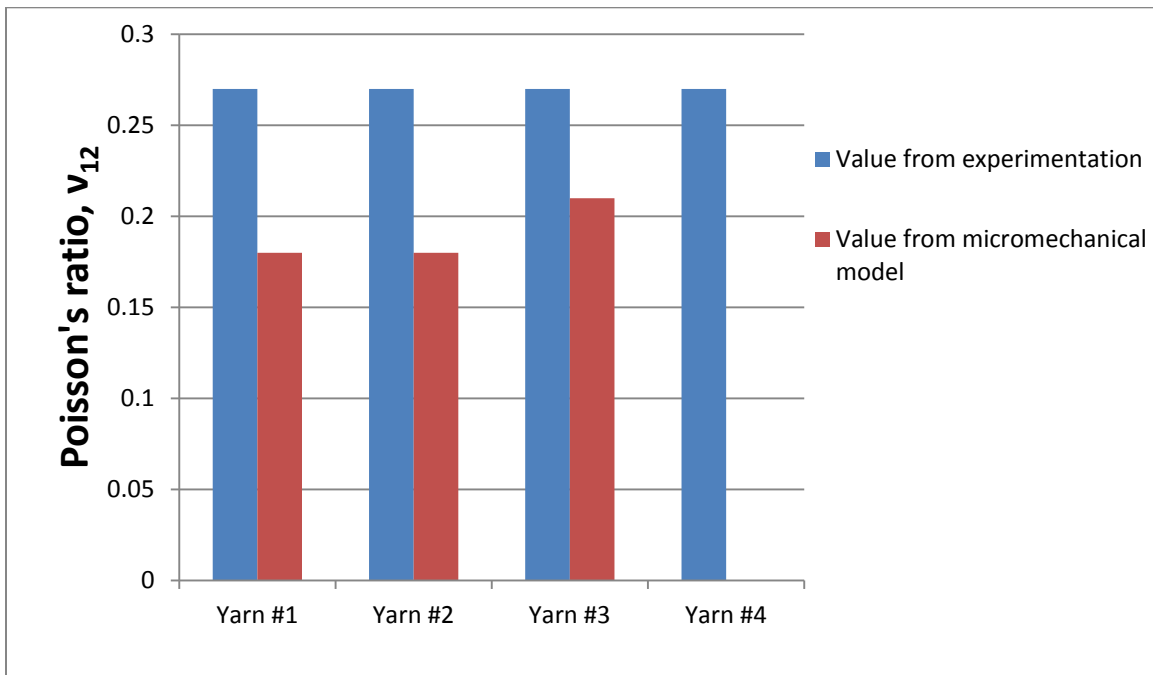
Figure 32: Comparison of Poisson's ratio, found experimentally and using micromechanical model

The engineering constants found using the micro mechanical modeling approach were compared against the values found experimentally in Figure 30 and Figure 31. While the Young's modulus

E_1 found experimentally was found to be within 10% error, the Poisson's ratios for the Yarns were predicted with 75 % accuracy. This error can be attributed to the error in finding the volume fractions, accounting for the strength properties of dry carbon tow and the textile fibers, the material properties (Poisson's ratio) of which are not easily available.

References

1. http://gertrude-old.case.edu/276/materials/21.htm

2. Kerstyn Comley, Norman A. Fleck, A micromechanical model for the Young's modulus of adipose tissue, *International Journal of Solids and Structures*, Volume 47, Issue 21, 15 October 2010, Pages 2982-2990, ISSN 0020-7683

3. Autar K. Kaw ,Mechanics of Composite Materials, Chapter 3,pg 151 to 171, CRC Press LLC

4. www.matweb.com, Search results for Nylon, Polyester and Kevlar^{TM}

5. Dr. Jeffrey Suhling, Mechanics of Composite Materials: Volume 1,pg 129, MECH 7360

6. Zheng-ming Huang, Micromechanical prediction of ultimate strength of transversely isotropic fibrous composites, *International Journal of Solids and Structures*, Volume 38, Issues 22–23, May–June 2001, Pages 4147-4172, ISSN 0020-7683

7. Zheng Ming Huang, Micromechanical strength formulae of unidirectional composites, *Materials Letters*, Volume 40, Issue 4, August 1999, Pages 164-169, ISSN 0167-577X, http://dx.doi.org/10.1016/S0167-577X(99)00069-5

8. Zheng-Ming Huang, Micromechanical life prediction for composite laminates, Mechanics of Materials, Volume 33, Issue 4, April 2001, Pages 185-199, ISSN 0167-6636

9. Zheng-Ming Huang, Simulation of the mechanical properties of fibrous composites by the bridging micromechanics model, *Composites Part A: Applied Science and Manufacturing*, Volume 32, Issue 2, February 2001, Pages 143-172, ISSN 1359-835X

10. D. Ivančević, I. Smojver, Micromechanical damage modelling using a two-scale method for laminated composite structures, Composite Structures, Volume 108, February 2014, Pages 223-233, ISSN 0263-8223

11. T. Parenteau, E. Bertevas, G. Ausias, R. Stocek, Y. Grohens, P. Pilvin, Characterisation and micromechanical modelling of the elasto-viscoplastic behavior of thermoplastic

elastomers, Mechanics of Materials, Volume 71, April 2014, Pages 114-125, ISSN 0167-6636

12. Ba Nghiep Nguyen, Mohammad A. Khaleel, A mechanistic approach to damage in short-fiber composites based on micromechanical and continuum damage mechanics descriptions, Composites Science and Technology, Volume 64, Issue 5, April 2004, Pages 607-617, ISSN 0266-3538

13. http://www.vectranfiber.com/BrochureProductInformation/TensileProperties.aspx, brochure with properties for Vectran^{TM} fiber

Chapter 6 Joints

Introduction

In the previous chapters we have developed the experimentation for finding the material constants of the composite yarns. The braiding of these yarns on to a circular mandrel results in final geometry of the open architecture tubes. This geometry is held together, once the structure is cured, by the overlaying of one yarn on top of the other. This results in the formation of a joint between the two yarns coming in contact with each other as shown in Figure 33.
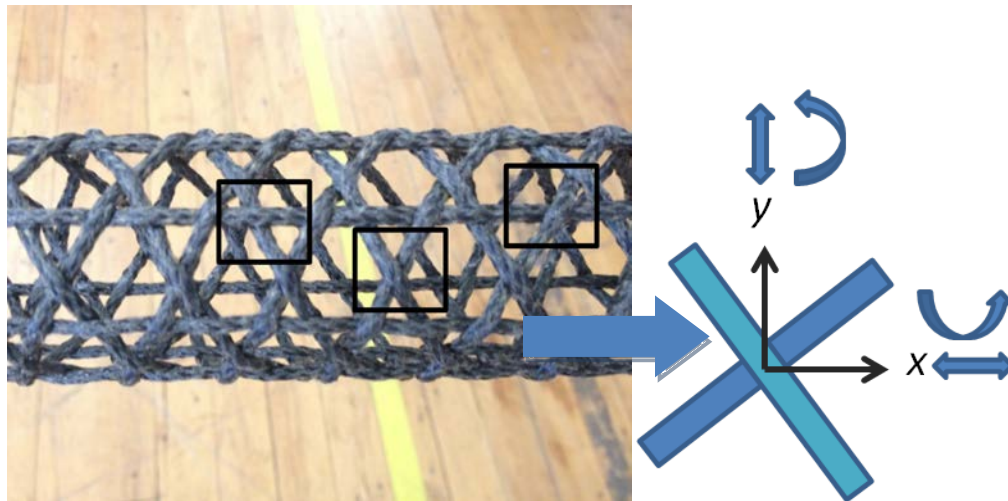

Figure 33: Joints on a open architecture tube with potential translations and rotations

The joints are formed by the resin present on or resin that exudes to the surface of each yarn. The formation of the joints restricts the linear and rotational degrees of freedom shown in Figure 33 ,thus increasing the axial and torsion stiffness of the tubes. For a tube made of 8 axial yarns and

8 helical yarns, 4 clockwise and 4 anti-clockwise, that is, a true triaxial braid, one unit cell of the tube contains 12 joints. 4 joints formed between the two helical yarns and the 8 joints formed between the axial and the helical yarns. The tangential and normal stiffness of each of these joints would add to axial, flexural, torsion stiffness and also to the stiffness in hoop direction of tube. If the joints are not formed then the yarns remain geometrically locked in a position and would be free to slide against each other under the application of load. Because of these reasons, it is very important to understand and investigate the quality of joints.

Following are the parameters were identified to affect the bond strength of the joints

1. Resin content in the yarn
2. Adhesive bond thickness
3. Amount of prepreg carbon fiber in the jacket of the yarn
4. Diameter of the yarn
5. Angle at which the joints are oriented

From the 5 parameters identified, adhesive bond thickness and angle subtended at the joints were identified as parameters that cannot be controlled given the current state of manufacturing. As the diameter of the yarn would increase, the amount of contact area of joint would increase which would result in better bond strength. Though, the diameter of the yarn more or less remained constant as the core of each yarn was the same (12K X 4 T700 prepreg).

Thus the resin content in the yarn and load to failure for the joints are the two parameters studied and discussed here on.

Resin Content in the Joints

The joints are formed by the resin present on the surface of the yarns. Also the high tension provided by the braiding machine allows for excess resin in the core to come out to the surface of the yarn. Initially, to improve the strength of the joints, excess resin was put on to the braided structure once the yarns were braided on mandrel [1]. This excess resin was believed to improve the bond strength of the joint. Though, the excess resin was believed to improve the bond strength, as will be shown in the Result section of this chapter, it increased the weight of the tube. Thus there was a compromise between the stiffness to weight ratio of the tube and the bond strength. Therefore, it was important to investigate the need to have excess resin to improve the

strength of the joint. For this purpose, initially the joints with excess resin and without the excess resin were observed under a scanning electron microscope.

Joint with Excess Resin

Joints , cut out from a tube made by putting excess resin after the first pre cure cycle were obtained under a scanning electron microscope.
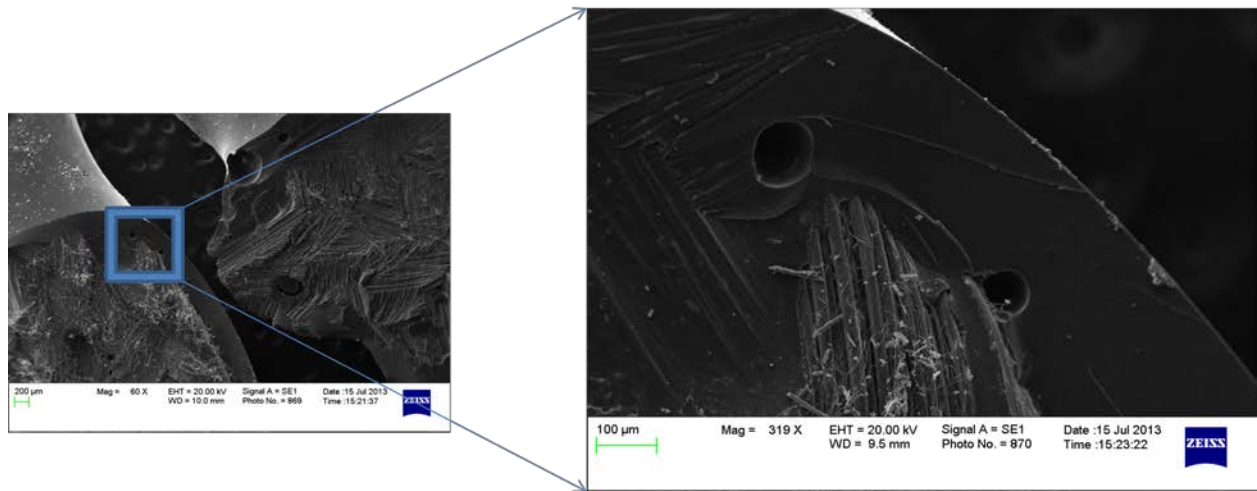

Figure 34: Micrograph of the interface of a broken joint

Figure 33 shows the image of a joint with excess resin. It can be seen that the excess resin put on the yarn, formed nearly a 0.25 mm thick layer around the yarn.

Adhesive thickness is an important parameter to the strength of the joint [8]. The load to failure is known to decrease with increase in adhesive thickness beyond a certain thickness [9,10,11]. The increase in the adhesive thickness decreases the brittleness of the joint and makes it more ductile.

In the case of the joints formed between the composite yarns, adhesive bond thickness is not a parameter that can be controlled, given the current manufacturing process. Also, the stiffness to weight ratio has been one of the strongest points of the open architecture tubes and a compromise on weight was seen to be more detrimental then the bond strength. Though, joints with and without excess resin have been tested and the results are reported in further sections. Also, yarn jackets with different textile fibers and varying amount of carbon content have been tested to find a characteristic which would be a leading indicator to the increase in bond strength.

Failure Modes for the Joints

Joint failure can be characterized in different ways depending on the location and direction of separation. Depending on location of failure, adhesive joints break in 3 different modes, cohesive failure mode, adhesive failure mode and adherend failure mode [2]. Figure 35 shows the three types of failure modes.

(a)Cohesive Failure mode   (b) Adhesive failure mode   (c) Adherend failure mode
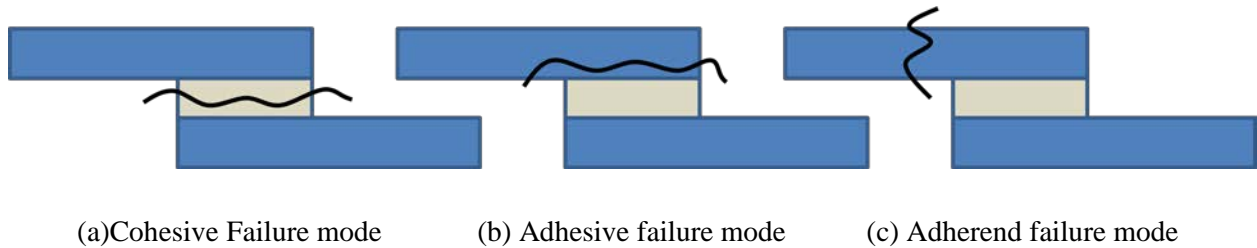
Figure 35: (a), (b) and (c) show different types of failure modes

Joints formed by the composite yarns have been found to fail by adhesive failure mode. Though, cohesive failure mode would have been the most desirable. The joints formed are also single lap joints. Failure of single lap joints have been studied extensively [3, 4]. Researchers have come up with near accurate numerical failure models [11]. Advanced optical methods like digital image correlation have been used to characterize the behavior of single lap joints [4]

Properties of the epoxy adhesive have been found experimentally [5] and used to make computational method to predict failure of adhesive joints [7]. Depending on the direction of separation 3 modes of debonding, mode 1 , mode 2 and mix mode debonding[15], have been studied [12,13,14].Depending on the nature of loading, bonded joints are known to fail in three most common ways. They are as follows:

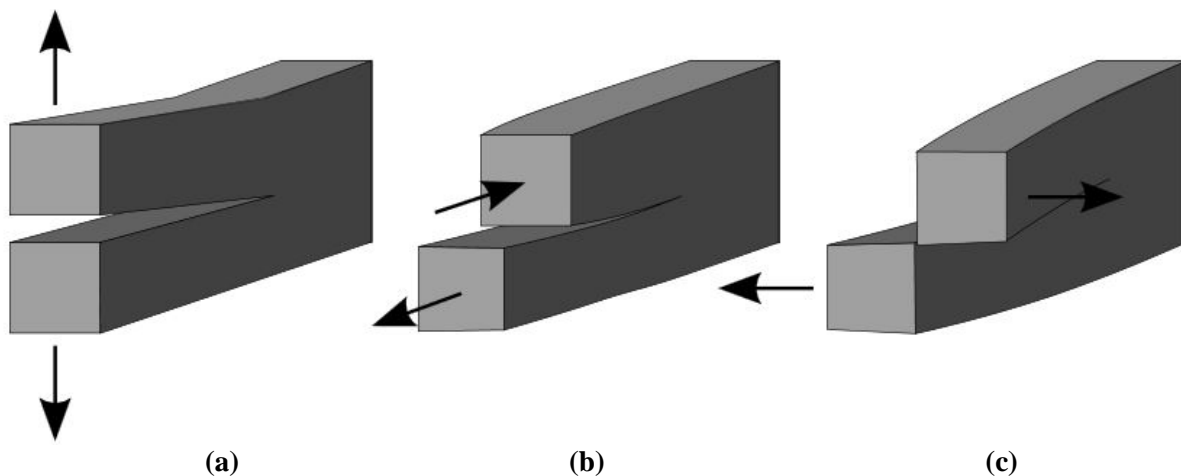**Figure 36: (a) Mode 1, (b) Mode2 and (c) mixed mode debonding modes**

Mode 1 debonding involves separation normal to the interface. Mode 2 de bonding involves slip tangent to the interface, though in plane. Mode 3 de bonding is slip tangent to the interface though, out of plane as shown in the Figure 35 above [15].

On an open architecture tube, a concentrated crushing load on one joint is known to cause Mode 1 type of debonding on the joint before and after the joint on which the load is applied. This force tries to displace the joint radially inwards as shown Figure 36, causing normal separation of the joints in the vicinity. Though, this load is reacted through the normal stiffness of the resin, K_{nn}. Since the contact area of the bond is small, approximately 4 mm^2, the joints are prone to mode 1 debonding.
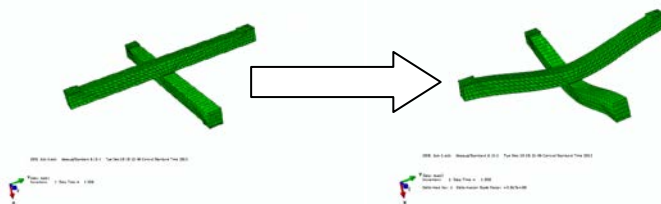

Figure 37: Mode 1 debonding on the tubes

The second most common loading scenario is the tube under a bending load. In this case, the yarns in the bottom half of the cross section is in tension and the ones in the top half are under

compression. At this point the axial yarns in the bottom half have a tendency to elongate under the tensile nature of the load. Though, the helical yarns have the same tendency, the helical geometry doesn't allow the yarn to extend to the same extent as the axial yarn does. This mismatch in axial component of the stiffness sets up shear stresses at the joint interface. Eventually, the joints are found to have a tangential slip in the plane of the joint, as shown in Figure 37. This type of failure is dependent on the tangential stiffness, K_{tt} of the resin is also known as the lap shear strength of the joint.
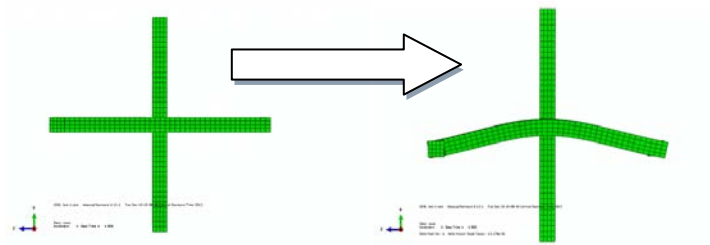
Figure 38: Initiation of Mode 2 debonding on the tubes

Thus it is important to know the crushing load and the bending load that cause each joint to break.

 Mode 1 type of debonding, involving separation normal to the interface has been tested and analyzed. Two goals were set for this study:

1. To evaluate the need of excess resin
2. To find the leading characteristic that governs the load to failure of the joint

Achieving these goals would aid the researchers make sound choice of the textile fibers and the amount and type of carbon fiber axials (prepreg or dry) in the jacket to improve the joints of the open architecture tube.

Results and Conclusion

A test fixture to cause mode 1 type of debonding was made. Figure 38 shows the fixture used for the test.
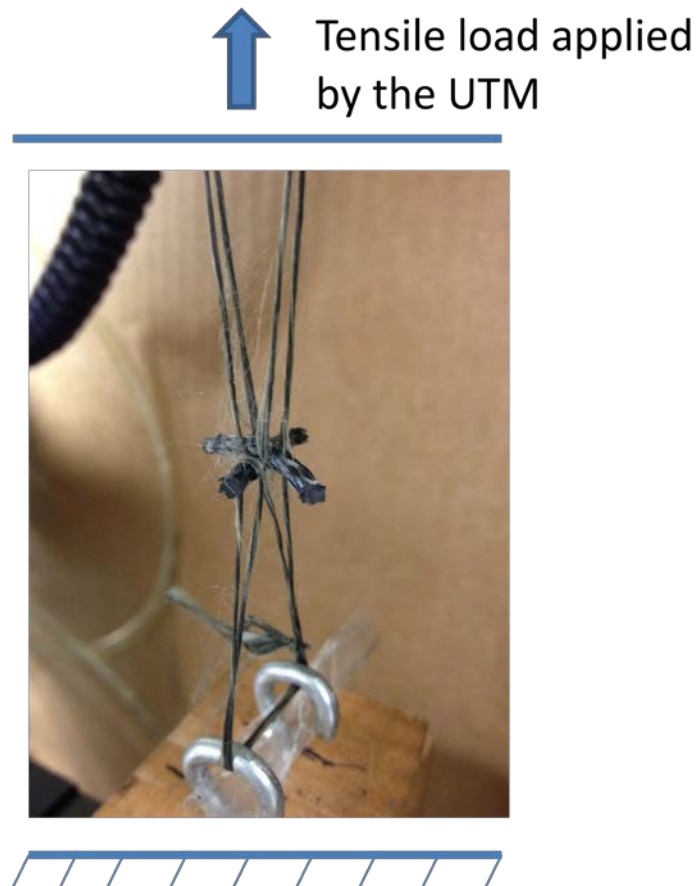
Figure 39: Test fixture of Mode 1 type of joint failure

Two wooden blocks, with hooks inserted in them were used to provide anchorage to the 2 inextensible strings that would hold the joint. Joints were cut from the tubes made, specifically for this study.

Results for Joints with Excess Resin

7 joints cut from a tube with excess resin were tested. Uni-axial tensile test conditions were defined for this test which caused the two yarns to separate normal to the bond interface. Loaf to failure was found for each of the joints. Figure 40 shows the
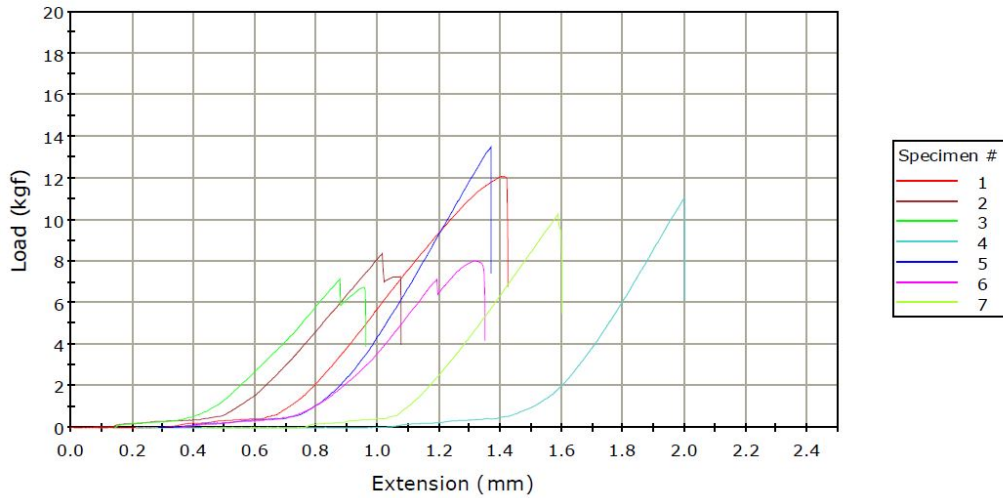
Figure 40: Graph of Load at Break Vs extension for join with excess resin

The loads to failure in Figure 39 are reported in

Table 15: Load at break for joints with excess resin

Joint number (Yarn with excess resin)	Load at break (Kgf)
1	12.06
2	8.35
3	7.13
4	11.02
5	13.75
6	8.05
7	10.18
Average	10.07

Results of Joints with no Excess Resin

Next tubes of yarns #2 were made without adding excess resin while curing the tube and the joints from these tubes were tested. The loads to failure for the 7 joints tested are reported in Table 13. The average load to failure for yarn #2 was found to be half of that of joints with excess resin. On analyzing the composition of yarn #2, it was found that, not much resin was available on the surface of the resin to form a joint. Yarn #2 had 4 prepreg carbon fiber tows and 4 dry carbon fiber tows as the axial fibers and 400 D Kevlar^{TM} as helical fibers in the jacket. Next, joints from the tube made of yarn #3 were tested. The loads to failure are reported in the table below.

Table 16: Loads to failure for yarn with and without excess resin

	Load at break (kgf) for joints with resin	Load at break (kgf) for joints without resin (yarn # 3)
1	12.06	18.95
2	8.35	13.07
3	7.13	16.26
4	11.02	16.59
5	13.75	19.29
6	8.05	23.66
7	10.18	13.93
Average	10.07	17.39

A comparison for the load at failure is made for the two types of yarns in Figure 40. The joints of this yarn had an average load to failure of 17 kgf, much more than that of joints with excess resin. Thus it was concluded that for yarns with similar diameter, similar cores, yarns with a no excess resin could be optimized further to make the joints perform better than their counterparts in the mode 1 debonding test.
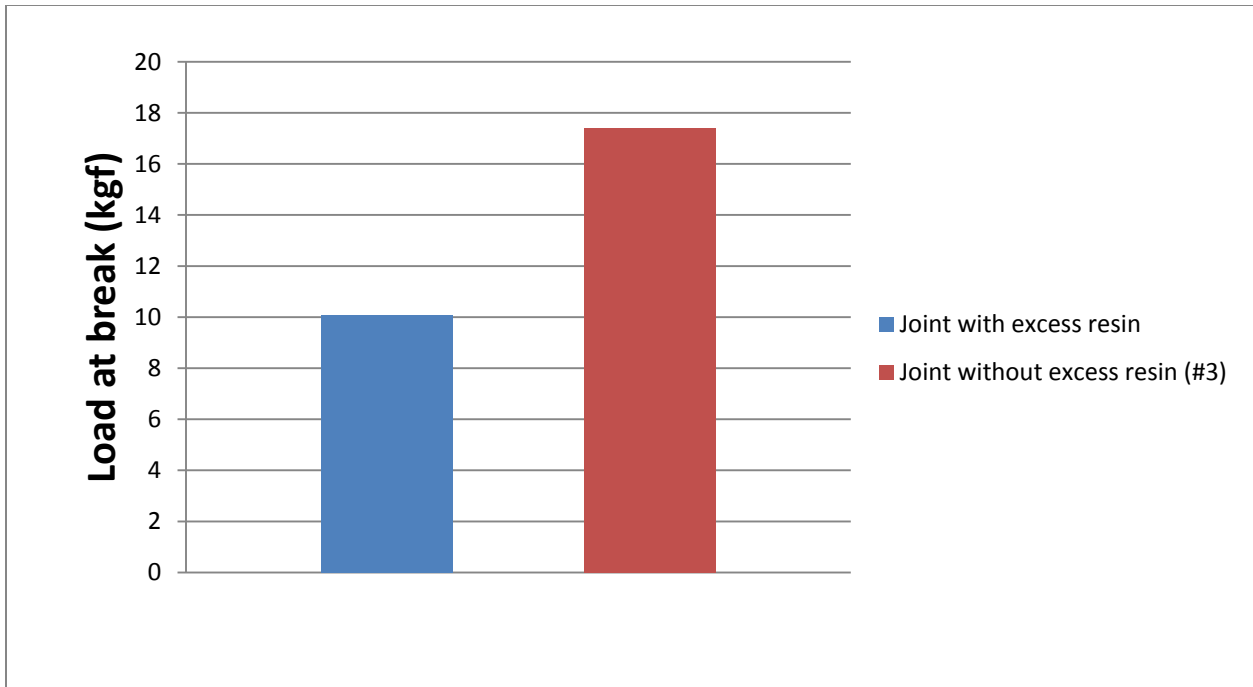
Figure 41: Comparison of loads to failure for joints with and without excess resin

This justifies the decision to keep the overall weight of the structure in mind and not add excess resin to improve strength. The difference between the #2 and #3 is in the amount of fiber in the jacket. While #2 has more amounts of fibers in the jacket, it has the same quantity if prepreg carbon tows in the jacket as compared to #3. Thus the fibers in the #3 had more amount of resin in the jacket to wet out the fiber than the #2. While the joints with excess resin performed better then joints of yarn #2, with the right changes in the jacket configuration, joints of yarn #3 performed better than former.

Yarn with Varying Jacket Architectures

Since joints of yarn #3 were found to have the highest load to failure, the make of the yarn #3 was further investigated to understand the parameter that resulted in better bond strength. For this purpose, 4 variants yarn #3, with varying denier count of tufted nylon and number of prepreg axials were made. The composition of each of these yarns is stated in Table 14.

Table 17: Composition of yarn #6, #7, #8 and #9

|	#6	#7	#8	#9
Core	48 K T700 prepreg	48 K T700 prepreg	48 K T700 prepreg	48 K T700 prepreg
Jacket Helicals (clockwise)	4 X 500 D nylon (carpet yarn)	4 X 1000 D nylon(carpet yarn)	4 X 1000 D nylon(carpet yarn)	4 X 500 D nylon(carpet yarn)
Jacket Helicals (anticlockwise)	4 X 500 D nylon(carpet yarn)	4 X 1000 D nylon(carpet yarn)	4 X 1000 D nylon(carpet yarn)	4 X 500 D nylon(carpet yarn)
Jackets Axials	4 X 3K T300 prepreg	4 X 3K T300 prepreg	8 X 3K T300 prepreg	8 X 3K T300 prepreg

Joints from the tubes made from each of these variants were tested. Figure 41 show the Load Vs Displacement graphs for #6 and #8.

Specimen 1 to 9
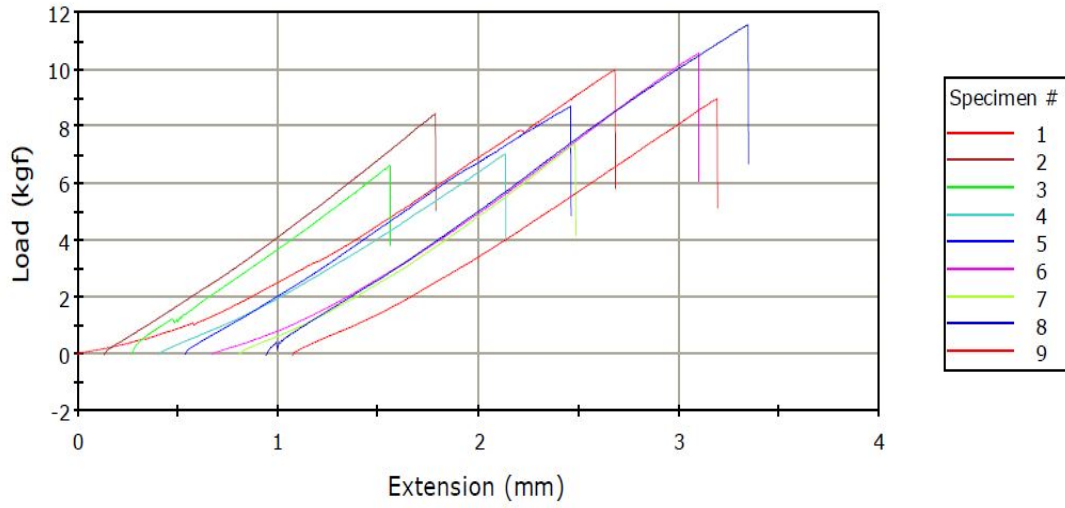
(a)

Specimen 1 to 9
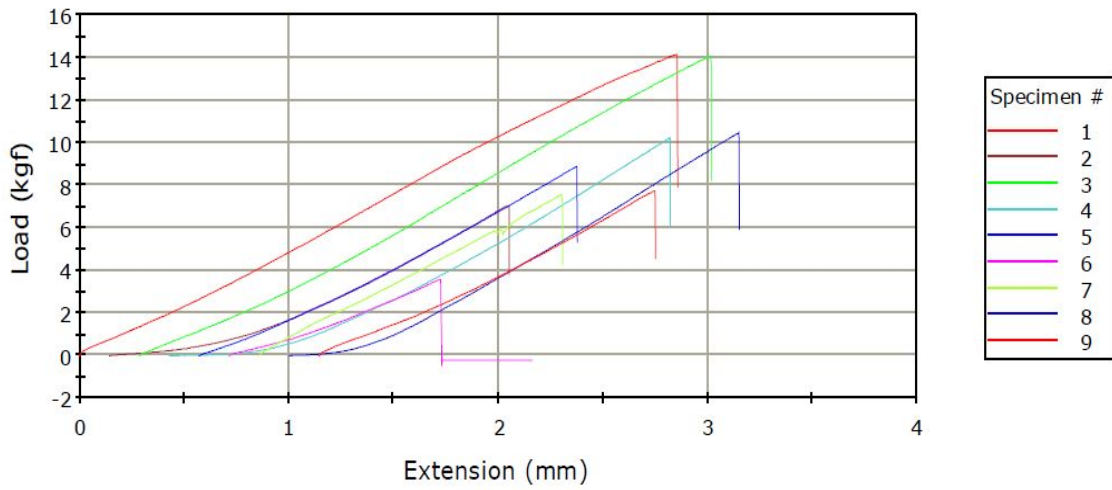
(b)

Figure 42: Load to failure Vs Extension graphs for (a) yarn #6 and (b) yarn #8

Similar graphs were obtained for joints of yarn #7 and yarn #9. The loads to failure for all the yarns are stated in Table 15.

Table 18: Loads to failure for joints of yarns #6, #7, #8 and #9

Type of yarn Sample no	Load to failure (kgf) #6	Load to failure (kgf) #7	Load to failure (kgf) #8	Load to failure (kgf) #9
1	9.99	5.76	14.15	12.16
2	8.46	10.10	7.05	13.96
3	6.63	7.69	14.0657	11.91
4	7.20	11.71	10.22	11.51
5	8.72	7.41	8.89	10.89
6	10.59	9.09	-	11.904
7	7.41	9.64	7.54	10.85
8	11.58	7.80	10.47	-
9	8.98	9.03	7.75	-
10	-	8.30	-	-
Average	8.84	8.97	10.01	11.88
Standard Deviation	1.646	1.647	2.804	1.047

Figure 42 shows a comparison of load to failures for yarns #6, #7, #8 and #9
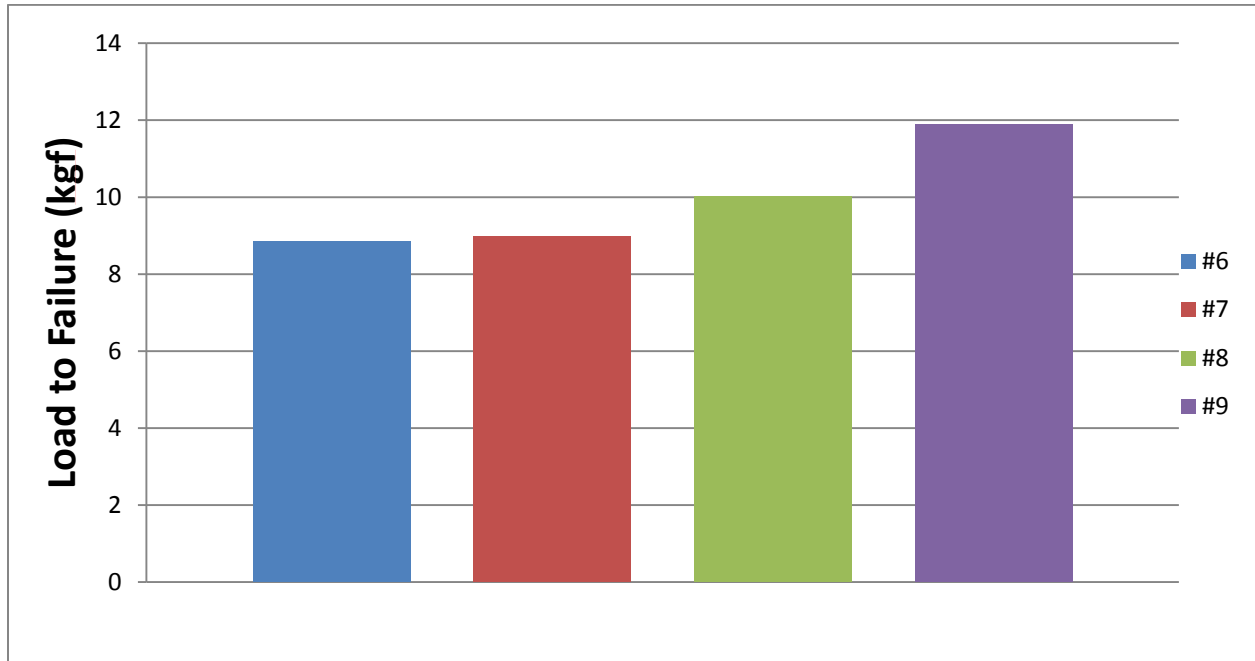
Figure 43: Comparison of load to failures for yarns #6, #7, #8 and #9

From the test data for the joints of yarns #6, #7, #8 and #9, it was seen that load to failure for #6 and #7 is nearly the same . This is because both these yarns have equal amount to axial prepreg carbon fiber in the jacket. Also the marginal increase in average load to failure for yarn #7 could be because of the slight increase in diameter of the yarn caused because of the 1000D tufted nylon.

 Yarn #8 and #9 have 8 prepreg carbon fiber axials instead of 4, thus more amount to resin available on the surface for bonding. Loads to failure for #8 and #9 were also found to be close. From this it could be concluded that for yarns similar to #3, more number of prepreg carbon fiber axials in the jacket improved the bond strength of the joints.

Preliminary Work on the Finite Element Analysis of the Joints

Introduction

In the previous section on the joints of the open architecture tubes, experimental method was developed and successfully used to find the load to failure for the joints in Mode 1 type of debonding. Usage of finite element methods to accurately predict the ultimate strength of the joints is very important. Much time and money can be saved by simulating yarns of different combinations of diameter, textile fibers and amount of carbon fiber prepreg in the jacket. FEM are widely being used in such applications. Advanced FEM packages available in the industry have made such methods, easy to implement, and less costly and less time consuming than performing experimentation.

Apart from experimentation, several techniques have been used by researchers to model debonding of different types of composites. X.Z.Lu and J.J. Jiang have studied debonding between FRP and concrete using finite element techniques [17]. They used ABAQUS for this analysis and modeled the interface between the two materials by making them share nodes at the interface. Researchers have modeled the matrix cracking in the fiber reinforced composites using extended vornoi cell FEM (Finite Element Method) [16,19]. Derewonko and team modeled the interface adhesive film between the bonded aluminum pieces using cohesive elements [6]. Debonding of concrete and FRP laminates as a function of FRP thickness has been studied using finite element analysis. It was found that the as the thickness of the adhesive increased the bond strength decreased [18]. Also micromechanical models have been developed to predict interfacial debonding in fiber reinforced composites [20].

Finite Element Modeling of Adhesive Joints

Work done by Derenwonko and team , on the strength assessment of adhesively bonded joints was found to be closely related to our research and problem at hand. They have developed a finite element model for mode 1 and mode 2 debonding of the adhesive joints formed between aluminium samples.

The work on the finite element modeling was done in two phases. The first phase is the prelimnary phase where a simple model depicting the correct geometry, material properties, elements, integration points, integration scheme , boundary conditions and loads is made. In this model the adhesive and the aluminium tabs are made to share nodes at the interface. The goal of this simulation was to evaluate the correctness of the model to depict the nature of the stresses at the adhesive. For example , shear debonding causes the elements in the adhesive film to come under shear load along its plane as shown in Figure 43.
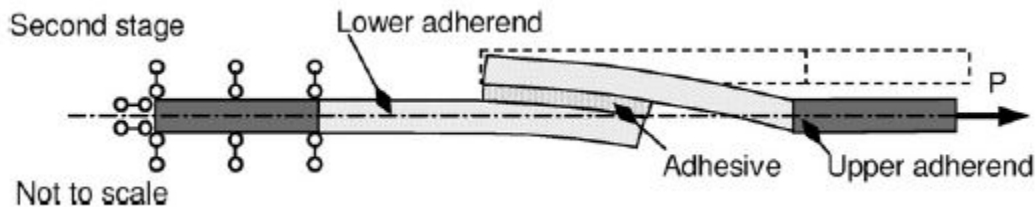

Figure 44: FEM model with boundary conditions for mode 2 type of debonding

Being able to obtain the same nature(shear debonding) in this prelimnary model helped the researchers to conclusively determine the boundary conditions and location of application of loads that would be used in the improved model. This model also helped them in determining the element type that would be used. Type of element, meshing technique, density of elements at various regions were decided at this prelimnary phase as well. This approach was found to be necessary as the improved model was based on a non-linear static contact analysis called the cohesive zone modeling. The cohesive zone model being a non linear analysis would take more computation time for each simulation to run and not having to work out different combinations and going in with a most of the variables determined saved the researchers a lot of time and efforts.

Considerable literature review was done on the implementation of the cohesive zone model which would be addressed in the section ahead.

Work done by Vinay Goyal and Team [7] and Derewonko and Team[6] also showed that Von Mises failiure governs the failure of adhesive joints . Load at which the elements representing the resin entered the plastic zone were tracked to indicate failure. It was noted that the work done by these researchers resulted in plastic strains towards the periphery of the adhesive films that initiated debonding.

Conclusions Made and Approach Selected

From the literature review it became clear the most appropriate modeling technique was the Cohesive zone modeling non linear static contact analysis. Inorder to effeiciently develop this nonlinear model prelimnary model with the resin and the yarn sharing nodes would have to be implemented. This model would help in zeroing in on various variuables like element type, element density, meshing technique, integration points, integration schemes, location on boundary conditions and loads.

On basis of the previous work done, it was decided that though the failure is caused at two locations at the same time, the complexity of the model would reduce greatly in terms of computation time and convergence difficulties if just one isolated joint was modeled. This would mean that accurate boundary conditions and loading would be of prime importance for the releveance of the isolated joint.

Prelimnary Model with Common Nodes

Two models , one representing mode 1 debondingand other representing mode 2 debonding, with defined made on ABAQUS. Figure 44 shows in detail, a model with shared nodes.
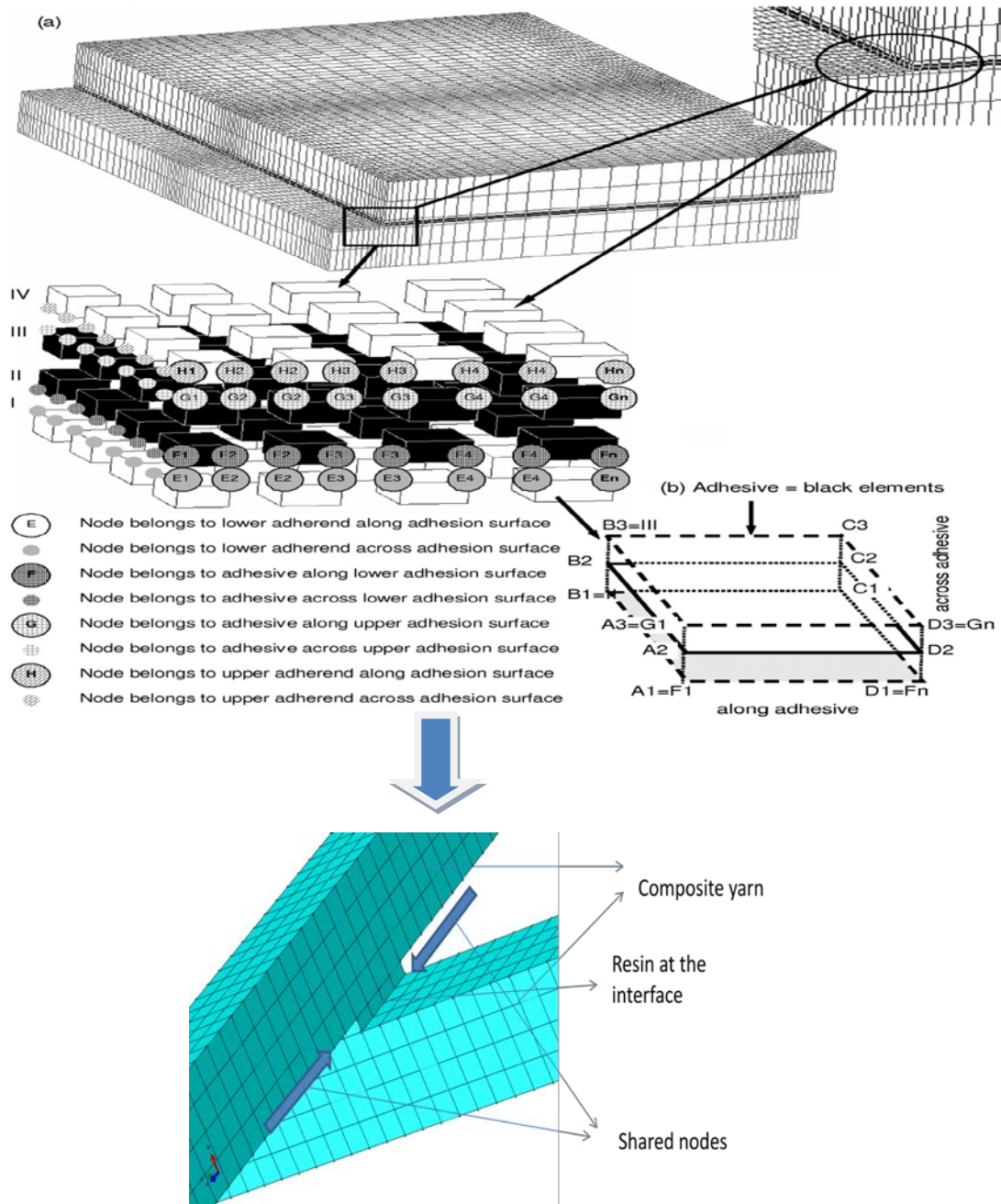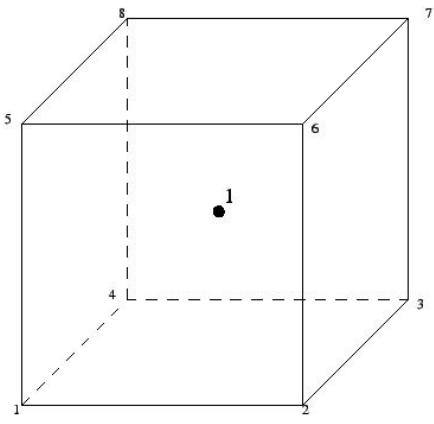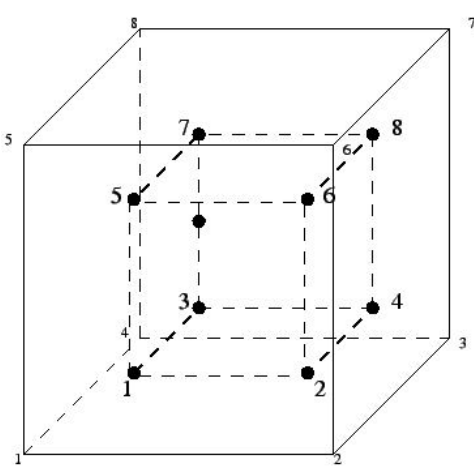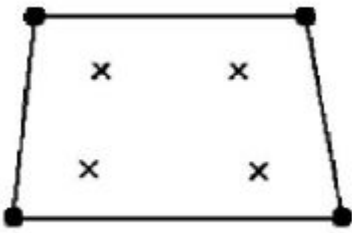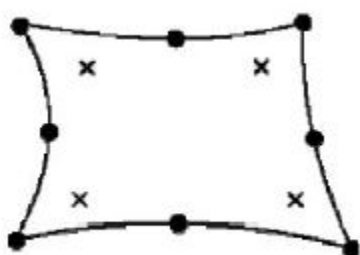

Figure 45: Model with shared nodes

Selection of Element Type

Solid elements and plate elements have been commonly used by researchers to model thin adhesive films and adherends. Plate elements are found to be good in modelling adhesive films of relatively small thickness, 100 microns and less. At such small thickness, solid elements tend to get stiffer and over predict the bending stresses induced in the adhesive films. Solid elements have been used to model adhesive with relatively greater thicknesses.

During the making of the open architecture tubes, the braided preforms are cured in two steps. At the first step just the braided structure is cured . At this stage, the prepreg braided yarn is cured. Before the second stage of curing, excess epoxy resin is put on the structure. Its this externally applied reisn which when vacuum bagged , seeps inside the joints to form an adhesive film. This externally applied resin also increses the thickness of the film that was earlier formed in the first stage of curing process. This initial work has only been done on joints with resin aapplied externally. For such joints the thickness of the film was found to be greater then 100 microns. With these considerations, it was decided that solid elements would be used to model the yarn and the resin. 8 node linear brick elements 20 node linear brick elements were studied and compared in Table 16 to decide which one of them was more suitable .Apart from the solid elements cohesive elements were further used in the cohesive zone model.

Table 19: Comparison of the 8 node linear brick elements 20 node linear brick element

Element Type	8 Node Brick element	20 node linear brick element
No. of nodes	8 nodes	20 nodes
Type of formulation and integration scheme	In modelling contact problems, first order interpolation elements with full integration scheme is adviced	In modelling contact problems, second order elements with reduced or full integration scheme are found to be good
	This element has 1X1X1 integration points and thus the values of stress are most accurate just at the center and not the edges	With 8 integration points, nearing the edges ,accurate values can be obtained at the places where maximum shear stress are found in our model and thus this element

On basis of the above comparisons a element C3D20R , 20 node brick element with qudratic formulation and reduced integration was selected.

A Study to Find the Appropriate Element Size

To find the optimum element size for the model a prelimnary model with a relatively big element size was initially made. This model was re run several times, each time element size smaller then the previous run. At the top corner node of the adhesive values of Von mises stress were tracked for each run.Its noted that the values of stiffness and stresses are calculated at the integration points withing the element and not the node, the values shown at the nodes are 75% averaged over the surrounding integration points.

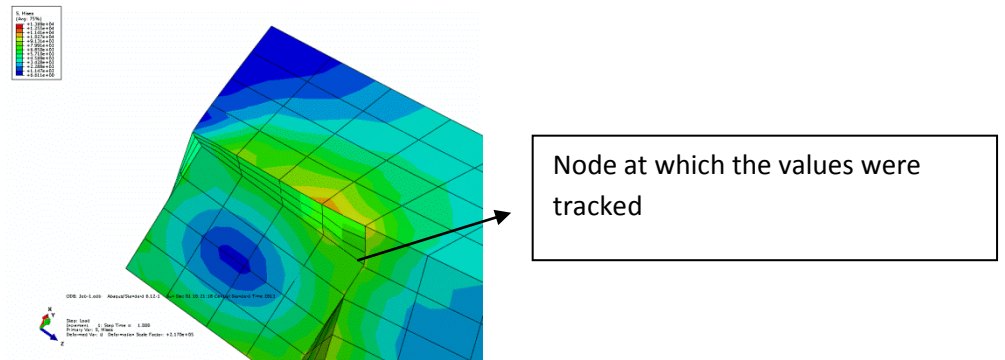Node at which the values were tracked

Figure 46: Location of node at which the Von Mises stress values were tracked

Figure 45 shows the location of the node at which the values of stress were tracked. From Figure 46 it was seen that the values of stress rose sharply when at the beginning when the element sizes were relatively big.
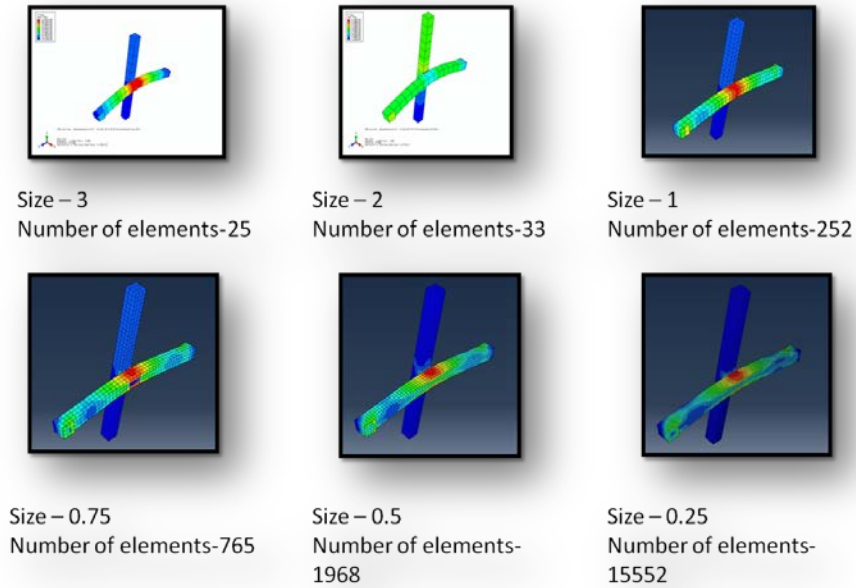
Figure 47: Models with different element sizes

Variation of Von Mises stress for different element sizes was obtained. A graph of Number of elements Vs Von Mises Stress at the selected node, shown in Figure 47 was plotted. The values started to get stable at around 1800 elements ie an element size of 0.7-0.6. It was inferred that on further reduction of the element size there was marginal increase in accuracy of the Von Mises stress. Thus an element size range of 0.7 to 0.6 was used in the advanced model. This exercise is done by researchers and professional FEM engineers before doing a nonlinear analysis as it allows them not having to rerun large nonlinear analysis , which usually take a lot of time , again and again to check for the correct element size and meshing techniques.

Figure 48: Number of elements Vs Von Mises stress

Material Properties, Boundary Conditions and Loads

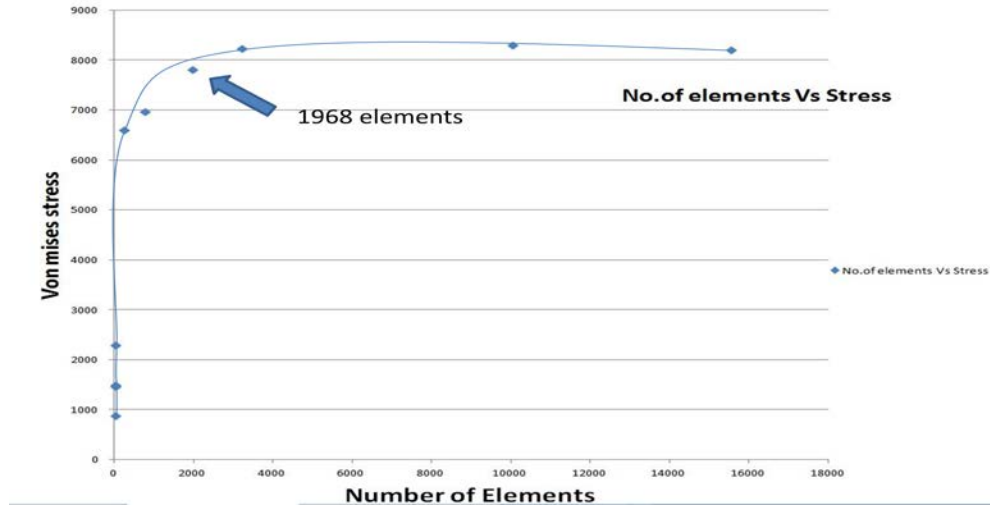The braided yarn is currently made in several different size of diameters ranging from 1.4 mm to 2.9mm, depending on the number of prepreg tows assembled to form the core of the yarn. In the regions where the joints are formed, the two yarns press against each other because of the tension produced by the braiding machine and a near flat rectangular joint interface is formed.

While modeling them for FE analysis several assumptions were made to reduce the complexity of the model, they are as follows:

1. The circular cross section yarn having 2mm diameter is simulated as a square cross section with sides of 2 mm

2. The resin at the interface is made to have a thickness of 0.25mm over a square cross section , with no resin coming out the joint and forming a radius at the periphery

3. Joints always form a close triangle, with three yarns crossing each other. While isolating a joint ,the presence of the other yarns on the isolated joint is made by modeling the top face of the resin patches at the bonded areas having fixed boundary conditions

4. Since the composite yarn is made of unidirectional carbon fiber tow , the yarn is modeled as an isotropic material with its E11 and Poisson's ratio in longitudinal direction defined

91

Material Properties

On basis of the assumptions made, the CFRP tow braided yarn was given linear material properties with its elastic modulus and Poisson's ratio defined along the axis of the material. The epoxy resin is a nonlinear material and thus apart from the elastic properties, Its yield stress and ultimate (plastic zone) stress to failure was defined.

CFRP braided yarn

Elastic modulus	97.36 x 10^3 MPa
Poisson's ratio	0.29

Epoxy resin

Elastic modulus	2,830 MPa
Poisson's ratio	0.35
Yield stress	68.95 MPa
Plastic stress	73. 06 MPa

Boundary Conditions and Loads

On basis of the assumptions made, fixed boundary conditions were applied to the faces of the joint where new joint would be formed. To simulate a pure normal and tangential debonding, all degrees of freedom except the ones in the motion would result in the respective debonding modes were restricted.
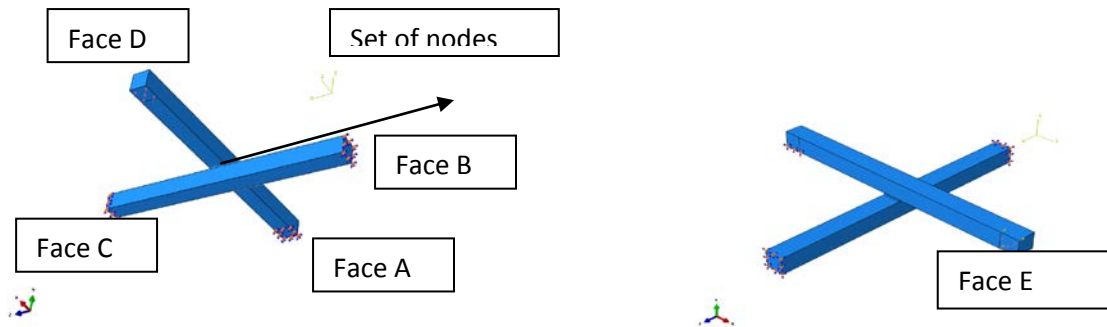
Figure 49: Locations of applied boundary conditions

Figure 48 shows the location of the boundary conditions and Table 17 shows the types of boundary conditions and load and where they were applied.

Table 20: Applied Boundary conditions and loads

Locations	Degrees of freedom locked
Face A	u1,u2,u3
Face B	u1,u2,u3
Face C	u1,u2,u3
Face D	Pressure load of 1000 N/mm^2
Face E	Pressure load of 1000 N/mm^2
Set of nodes	u3, rotation along x and y

Cohesive Zone Model

This method is used to model the behavior between the adhesive and the adherend in the project. The concept of the this technique and how it is implemented in ABAQUS is described in this section

Theory

Non-linear problems (contact and plasticity) which are found during the analysis require an iterative penetration method to be solved. Using this procedure, the iteration process is done simultaneously to satisfy both the contact constraints and global equilibrium using Newton–Raphson procedure. The contact condition is based on the true surface geometry. A Coons surface is used in order to improve the geometric representation in calculating the normal. The surface is expressed in a four-dimensional homogeneous coordinate space by

$$P(u,v) = \frac{\sum_{i+1}^{n+1} \sum_{j=1}^{m+1} B_{i,j} h_{i,j} N_{i,k}(u) M_{j,l}(v)}{\sum_{i+1}^{n+1} \sum_{j=1}^{m+1} h_{i,j} N_{i,k}(u) M_{j,l}(v)}$$

Equation 31

where the B are 4D homogeneous defining polygon vertices, $N_{i,k}$ and $M_{j,k}$ are non-rational B-spline basis function, $h_{i,j}$ is a homogeneous coordinate. For given parameters u and v in a local system, the location (x,y, z) in a three dimensional space, the first derivative and the second derivative, are calculated . A kinematics' boundary condition is continuously changing because the normal can change from iteration to iteration:

$$(\Delta u_{normal})^0 = v.n$$

Equation 32

$$(\Delta u_{normal})^i = v.n_1 - v.n_0$$

Equation 33

where the subscripts represent the iteration number.

When contact occurs, a reaction force associated with the node in contact balances the internal stress of the elements adjacent to this node. The value of an internal stress is the maximum residual force at node n divided by the contact area of node n. After the node comes into contact with the other node, it is possible for it to separate in subsequent iteration or increment. Therefore node should separate when a tensile force or normal stress exceeds the surface tension. Such an approach allows determining and comparing the forces and stressing distribution along and across the adhesive and adherend bond lines.

Theoretical Implementation in ABAQUS

The cohesive zone model has been implemented in the commercial finite element package, ABAQUS. In particular, cohesive elements are defined along the potential paths of crack growth (e.g., a bimaterial interface). The constitutive properties of the cohesive elements are specified in terms of the traction-separation law. Several types of traction-separation laws have been implemented, and self-developed user subroutines may be incorporated for the cohesive elements with non-standard traction-separation laws. In the present study, we adopt the energy-based failure criterion:

Software Implementation

While setting up the cohesive zone model for energy criterion, we need to define firstly the faces along which contact would be made. Next, node to surface type of contact was defined. Here nodes on the resin surface are selected to contact the surface on the yarn through the cohesive element. This procedure sets up the initial interactions definition in ABAQUS.

Now the properties of the energy based criterion are defined. This is done in 2 steps

Damage Initiation properties

Maximum normal stress = 60MPa

Maximum shear 1 stress= 60 Mpa

Maximum shear2 stress= 0

Damage evolution Properties

Normal fracture energy= 0.1 J/ mm^2

1st shear fracture energy=0.1 J/mm^2

2nd shear fracture energy=0

These above mentioned parameters are to be found by basic lab experimentation on the samples and at the current phase, these values are taken from web and the true values would be used in future once the experimentation would be done.

Results

Results for Mode 1 Debonding
The primary objective of this study was to find the load capacity of the joint mode 1 type of debonding. The analysis was successfully run and from the results obtained. Figure 49 shows the debonding of the joint, before and after the load was applied.

Deformed Images

(a)   (b)
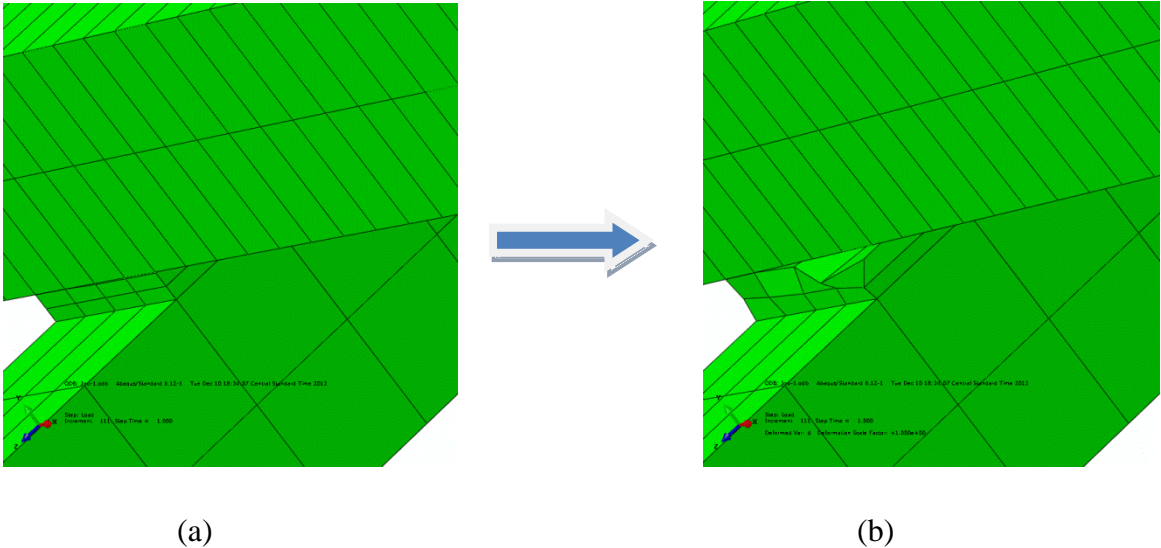
Figure 50: (a) Mode 1 debonding, before load applied; (b) Mode 1 debonding, after load applied

Load Vs displacement graph was plotted for the node which underwent debonding.
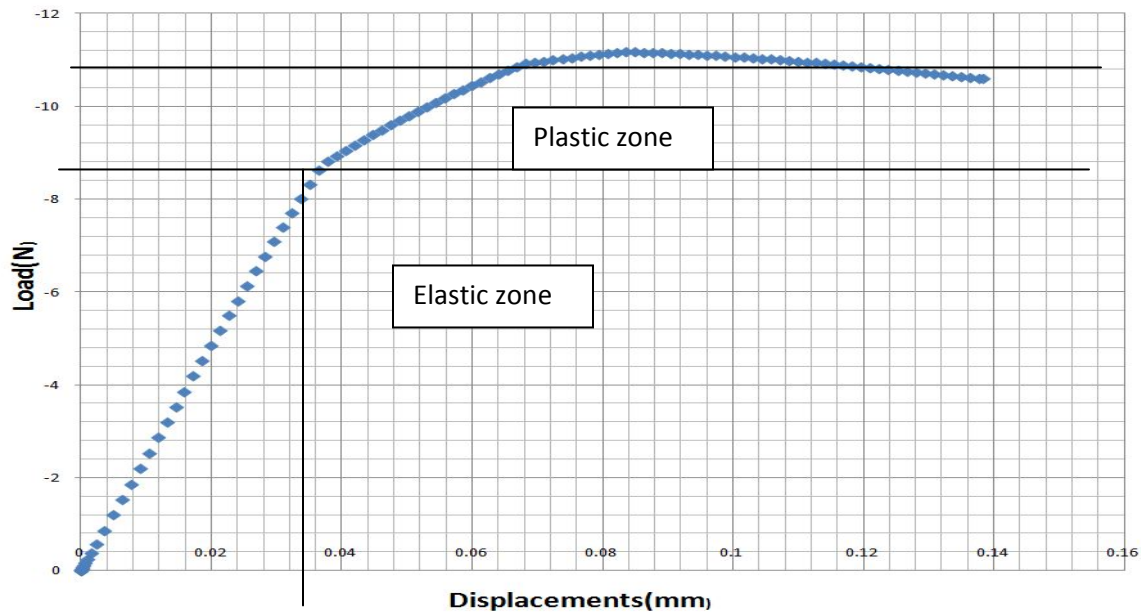

Figure 51: Displacement Vs Load graph for mode 1 debonding

From the graph above the load capacity of the joint was found to be 8.81 N. At this load the joint yielded for the first time. The displacement gradient increased rapidly after this point and thus the resin and fiber interface was plastically deformed beyond this point. Then at load 10.91 N, the displacement gradient almost flattened out, thus with no increase in load the displacement kept on increasing. The first yielding occurred at a displacement of 0.03 mm which corresponds to 12% elongation before failure.

Results for Mode 2 Debonding

In this model a tangential slip was occurred at the interface. A in plane shear failure occurred at the interface.

Deformed images

(a)   (b)
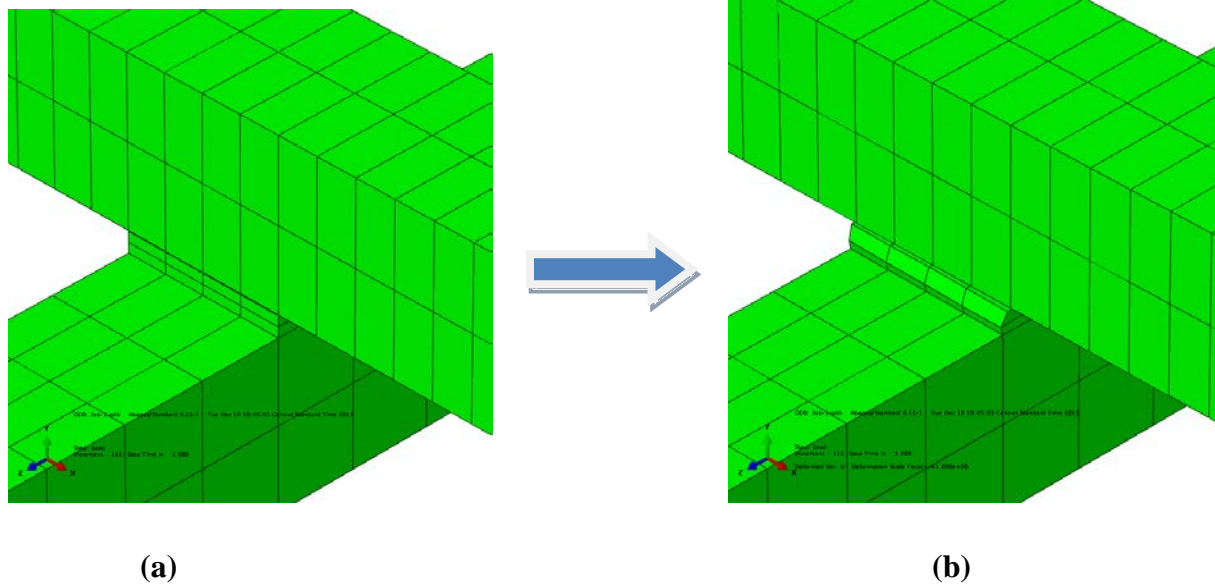
Figure 52: (a) and (b) represent Mode 2 debonding, before and after application of load

In this model a tangential slip was occurred at the interface. Again a displacement Vs load graph was plotted at the corner node on the resin where the debonding started.
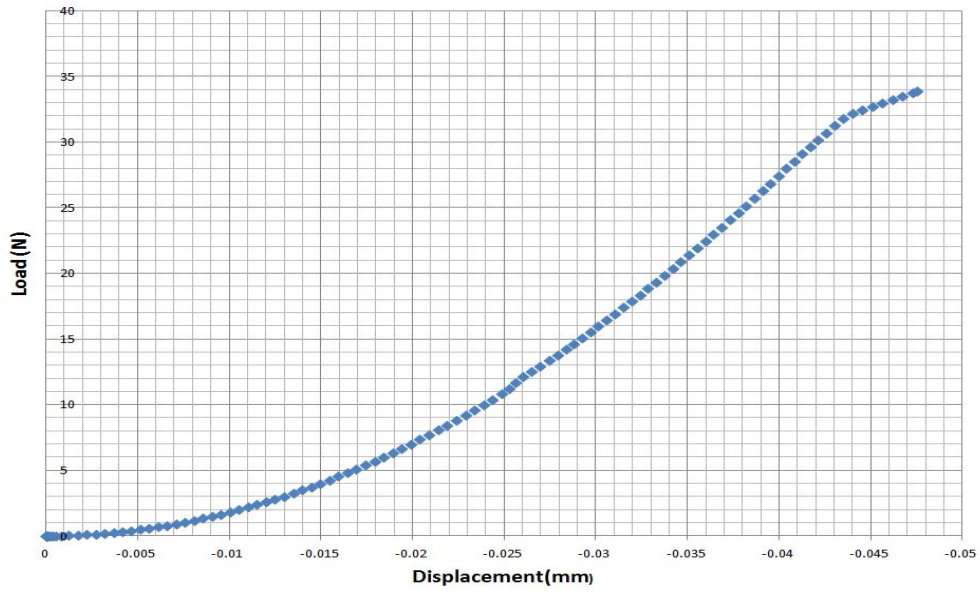
Figure 53: Displacement Vs Load graph for mode 2 debonding

It is seen that the slope of the graph changed drastically at a load of 31 N. Beyond this point again the gradient of displacement started increasing rapidly and thus it was inferred that this load was the loading capacity of the joint.

Conclusions

It was seen that the most strained element in both the modes of debonding remained the corner most element on the side opposite to where debonding started. Apart from that, the values for load at break obtained for the 2 types of failure modes do not mean anything at the current stage of research. The goal of our initial work was just to develop a methodology for simulating the joints using Cohesive Zone modeling technique and narrow down vital parameters like type of element, element size and perhaps find critically stressed regions of the joint as shown in Figure 53.
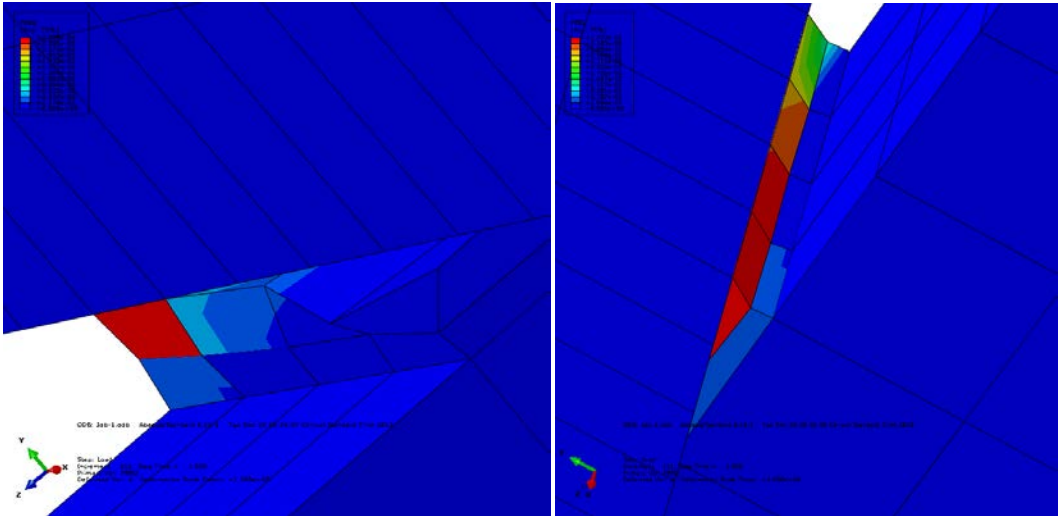

Figure 54: Mode 1 & Mode 2: Corner elements on the side opposite to the debonding side

References

1. D.Branscomb, " Minimal Weight Composites Utilizing Advanced Manufacturing Techniques ", PhD dissertation, Auburn University, 2012

2. N.M. Rahman, C.T. Sun, Strength Calculation of Composite Single Lap Joints with Fiber-Tear-Failure, *Composites Part B: Engineering*, Available online 22 March 2014, ISSN 1359-8368

3. Kwang-Soo Kim, Yeong-Moo Yi, Gwang-Rae Cho, Chun-Gon Kim, Failure prediction and strength improvement of uni-directional composite single lap bonded joints, *Composite Structures*, Volume 82, Issue 4, February 2008, Pages 513-520, ISSN 0263-8223

4. A.J. Comer, K.B. Katnam, W.F. Stanley, T.M. Young, Characterising the behaviour of composite single lap bonded joints using digital image correlation, *International Journal of Adhesion and Adhesives,* Volume 40, January 2013, Pages 215-223, ISSN 0143-7496

5. K.-D Bouzakis, I. Tsiafis, N. Michailidis, A. Tsouknidas , Determination of epoxy resins' mechanical properties by experimental computational procedures in tension, *Proceedings of the 3rd International Conference on Manufacturing Engineering (ICMEN)*, 1-3 October 2008

6. Agnieszka Derewonko, Jan Godzimirski, Krzysztof Kosiuczenko, Tadeusz Niezgoda, Andrzej Kiczko, Strength assessment of adhesive-bonded joints, *Computational Materials Science*, Volume 43, Issue 1, July 2008, Pages 157-164, ISSN 0927-0256

7. Vinay K. Goyal, Eric R. Johnson, Vijay K. Goyal, Predictive strength-fracture model for composite bonded joints, *Composite Structures*, Volume 82, Issue 3, February 2008, Pages 434-446, ISSN 0263-8223

8. Lijuan Liao, Chenguang Huang, Toshiyuki Sawa, Effect of adhesive thickness, adhesive type and scarf angle on the mechanical properties of scarf adhesive joints*, International Journal of Solids and Structures*, Volume 50, Issues 25–26, December 2013, Pages 4333-4340, ISSN 0020-7683

9. Wei Xu, Yueguang Wei, Influence of adhesive thickness on local interface fracture and overall strength of metallic adhesive bonding structures, *International Journal of Adhesion and Adhesives*, Volume 40, January 2013, Pages 158-167, ISSN 0143-7496

10. A. Moradi, D. Leguillon, N. Carrère, Influence of the adhesive thickness on a de bonding– An asymptotic model, *Engineering Fracture Mechanics*, Volume 114, December 2013, Pages 55-68, ISSN 0013-7944

11. S. Feih, H.R. Shercliff, Composite failure prediction of single-L joint structures under bending, *Composites Part A: Applied Science and Manufacturing*, Volume 36, Issue 3, March 2005, Pages 381-395, ISSN 1359-835X, http://dx.doi.org/10.1016/j.compositesa.2004.06.021

12. Laura De Lorenzis, Giorgio Zavarise, Modeling of mixed-mode de bonding in the peel test applied to superficial reinforcements, *International Journal of Solids and Structures*, Volume 45, Issue 20, 1 October 2008, Pages 5419-5436, ISSN 0020-7683

13. Laura De Lorenzis, Dilum Fernando, Jin-Guang Teng, Coupled mixed-mode cohesive zone modeling of interfacial de bonding in simply supported plated beams, *International Journal of Solids and Structures*, Volume 50, Issues 14–15, July 2013, Pages 2477-2494, ISSN 0020-7683

14. Chien Nguyen, Alan J. Levy, An exact theory of interfacial de bonding in layered elastic composites, *International Journal of Solids and Structures*, Volume 46, Issue 13, 15 June 2009, Pages 2712-2723, ISSN 0020-7683

15. Ansys Contact Technology Guide, Section 12, pg 132, Release 12.1,2009

16. S. Li, S. Ghosh, Modeling interfacial de bonding and matrix cracking in fiber reinforced composites by the extended Voronoi cell FEM, *Finite Elements in Analysis and Design*, Volume 43, Issue 5, March 2007, Pages 397-410, ISSN 0168-874X

17. X.Z. Lu, J.J. Jiang, J.G. Teng, L.P. Ye, Finite element simulation of de bondingin FRP-to-concrete bonded joints, *Construction and Building Materials*, Volume 20, Issue 6, July 2006, Pages 412-424, ISSN 0950-0618

18. Feifei Lu, Ashraf Ayoub, Evaluation of de bonding failure of reinforced concrete girders strengthened in flexure with FRP laminates using finite element modeling, *Construction and Building Materials*, Volume 25, Issue 4, April 2011, Pages 1963-1979, ISSN 0950-0618

19. Somnath Ghosh, Yong Ling, Bhaskar Majumdar, Ran Kim, Interfacial de bonding analysis in multiple fiber reinforced composites, *Mechanics of Materials*, Volume 32, Issue 10, October 2000, Pages 561-591, ISSN 0167-6636

20. A. Caporale, R. Luciano, E. Sacco, Micromechanical analysis of interfacial de bonding in unidirectional fiber-reinforced composites, *Computers & Structures*, Volume 84, Issues 31–32, December 2006, Pages 2200-2211, ISSN 0045-7949

Chapter 7 Conclusions

Over the course of our work, several important conclusions were drawn. The conclusions mentioned below are the major finding of this research. These conclusions have been described in details in the previous chapters.

1. The results of the tensile tests on yarns of different jacket architectures showed a trend of increasing values of Young's modulus as the (prepreg) carbon content in the yarn increased.

2. It was found that the Hertzian-contact model used for calculating transverse modulus of the yarns could yield values of modulus with good accuracy. This was observed from the validation tests performed on nylon 6,6 samples with known values of transverse modulus

3. Micromechanical model, specific to the braided composite yarn, can accurately predict the Young's modulus along the axis. Literature review showed that micromechanical model for finding transverse modulus and in plane shear modulus was not reliable in predicting those values respectively.

4. Bond strength of the joints can be improved further, beyond the bond strength of the joint with excess resin. This can be done by controlling the amount of resin available for bonding on the surface of the yarn.

5. With the increase in prepreg carbon fiber tows in the jacket, the bond strength of the joints improves. This was accredited to the increased content of resin available for bonding on the surface of the yarn.

   It was noted that yarns with highest longitudinal stiffness may or may not yield joints with good strength. The strength of the joint is majorly dependent on the jacket architecture, resin available on the surface for bonding and diameter of the yarn.